ENCLOSURE 2

MFN 09-106

Request for Additional Information Response for the PRIME Model for Analysis of Fuel Rod Thermal – Mechanical Performance

Non-Proprietary Information

IMPORTANT NOTICE

This is a non-proprietary version of Enclosure 1, which has the proprietary information removed. Portions of the document that have been removed are indicated by white space with an open and closed bracket as shown here [[ ]].

NEDC-33256P – Technical Basis

RAI-1 (full text)

Table 2.1 of NEDC-33256P lists the limits of application that are being requested for PRIME. Data have not been provided in the submittal used to qualify PRIME to some of these levels. Please address the following areas where data is lacking or propose new limits of applications for PRIME for which data is available.

a. Discuss the data that are available for fuel densities greater than 97.5% TD (it is noted that past experience has shown difficulty in fabricating UO2 fuel with densities > 97.5% TD).

b. Discuss the data that are available for fuel temperatures greater than fuel melting along with code/model comparisons to this data including cladding deformation, fuel melt radius, and FGR.

c. Discuss the data that are available for cladding temperatures greater than 752 °F along with code/model comparisons to this data including cladding creep and deformation.

d. Discuss the data that are available for fuel with grain sizes greater than 15 microns along with code/model comparisons to fission gas release, fuel creep and cladding deformations from power ramp data.

e. Please provide a plot showing LHGR vs. burnup for rods that PRIME has been compared to with each rod shown with a different symbol. Also discuss what experience you have with high burnup fuel under AOO and accident conditions (if the code is applied to a specific accident).

f. This table does not specify the cladding type that PRIME should be limited to. Please list the cladding alloy(s) and type(s) (e.g. RXA or CW-SRA, etc.) that have sufficient qualification data and that the code may be applied to.

RAI-1.a (full text)

Discuss the data that are available for fuel densities greater than 97.5% TD (it is noted that past experience has shown difficulty in fabricating UO2 fuel with densities > 97.5% TD).

Response:

GNF concurs with the comment. The nominal density for current product fuel is 97-97.5 %TD. Thus, GNF has limited experience for fuel with greater than 97.5 %TD. Some short fuel segments with 98-99 %TD have been specially fabricated for irradiation testing. This experience is summarized in Table 1.1.

Table 1.1: Irradiation Experience with Fuel Pellet Density Greater Than 97.5% TD

Qualification Parameter	Rod Identification	Exposure, GWd/MTU	LHGR, kW/ft	Pellet OD, inch	Pellet Density, %TD	Description
Fuel Centerline Temperature	[[				-------	NEDC-33257P, Section 2.1
Diametral & Axial strain					---	Rod Irradiated in Test Reactor, NEDC -33257P, Section 3.1

Fission Gas Release					------	NEDC -33257P, Section 3.1 & Section 4.1

					---------]]	

RAI-1.b (full text)

Discuss the data that are available for fuel temperatures greater than fuel melting along with code/model comparisons to this data including cladding deformation, fuel melt radius, and FGR.

Response:

Current fuel design SAFDLs requires no fuel melting. However, GNF has [[

]]Direct temperature measurements are not available from these tests, but grain growth and melt

radius is available, as well as cladding deformations. The test database is summarized in Table 1.2. Figure 1.1 shows irradiation histories for some of these rods. Figure 1.2-1.4 show PRIME prediction of diametral strain as a function of melting volume fraction, fuel centerline temperature and fuel normalized melting radius, respectively.

Table 1.2 Rods Irradiated in Test Reactor

ROD_ID	Exposure (MWd/t)	Power (kW/ft)
GE_S317_IL	[[	
GE_S317_IU		
GE_S317_KL		
GE_S317_LL		
GE_S317_AL		
GE_S317_AU		
GE_S317_BL		
GE_S317_CL		
GE_S317_CU		
GE_S317_DL		
GE_S317_DU		
GE_S317_EL		
GE_S317_EU		
GE_S317_FU		
GE_S317_GL		
GE_S317_GU		
GE_S317_HU		
GE_S317_LU		
GE_S317_MU		]]

[[ ]]

Figure 1.1: Irradiation histories for the rods irradiated in Test Reactor

[[ ]]

Figure 1.2: PRIME prediction of diametral strain as a function of melting volume fraction for rods irradiated in Test Reactor

[[ ]]

Figure 1.3: PRIME prediction of diametral strain as a function of fuel centerline temperature for rods irradiated in Test Reactor

[[ ]]

Figure 1.4: PRIME prediction of diametral strain as a function of fuel normalized melting radius for rods irradiated in Test Reactor

RAI-1.c (full text)

Discuss the data that are available for cladding temperatures greater than 752 °F along with code/model comparisons to this data including cladding creep and deformation.

Response:

At higher temperature [[ ]]PRIME calculates the cladding plastic deformations by using the stress strain relation as described in Section 4.1.3 of NEDC-33256P. This stress strain relation is also used to calculate creep deformation at high temperature, as described in Section 5.6.3 of NEDC-33256P. Comparison of the PRIME creep model with the out of reactor high temperature creep data is shown in Figures 1.5 to 1.8.

[[ ]]

Figure 1.5: Comparison of PRIME Model with the Out of Reactor Zircaloy Clad Uniaxial Creep Measurements (Reference 1.c.1).

[[ ]]

Figure 1.6: Comparison of PRIME Model with the Out of Reactor Zircaloy Channel Strip Uniaxial Creep Measurements (Reference 1.c.2).

[[ ]]

Figure 1.7: Comparison of PRIME Model with the Out of Reactor Zircaloy Channel Strip Uniaxial Creep Measurements (Reference 1.c.2).

[[ ]]

Figure 1.8: Comparison of PRIME Model with the Out of Reactor Zircaloy Channel Strip Uniaxial Creep Measurements (Reference 1.c.2).

References:

[1.c.1] Pelloux, RM, Ballinger, R and Lucas, G.,"The Effects of Anisotropy and Irradiation on the Deformation Behavior of Zircaloy-2", EPRI NP-782, January 1979.

[1.c.2] Woodford, DA, "Creep Analysis of Zircaloy-4 and its Application in the Prediction of Residual Stress Relaxation" , J. Nucl. Mat. 79 (1979) 345-353.

RAI-1.d (full text)

Discuss the data that are available for fuel with grain sizes greater than 15 microns along with code/model comparisons to fission gas release, fuel creep and cladding deformations from power ramp data.

Response:

Table 1.3 summarizes the PRIME qualification database that includes fuel pellets with (initial) grain size larger than 15 microns. Figures 1.9-1.11 show comparisons of PRIME model predictions to FGR data for rods with grain size larger than 15 microns. Figures 1.12-1.15 show comparisons of PRIME model predictions to cladding deformation data from normal operation and from power ramped rods and for the rods with grain size larger than 15 microns.

Table 1.3: PRIME Qualification Database with Fuel Pellet Grains Larger than 15 microns.

Qualification Parameter	Number of rods		
	Total	Grain size > 15 micron	Percent
Fuel Temperature	[[		
Diametral Deformation			
Diametral Deformation (ramp)			
Axial Deformation			
Axial Deformation (ramp)			
Fission Gas Release			
Rod Internal Pressure			]]

[[ ]]

Figure 1.9: Predicted vs. Measured FGR for Fuel Rods with Grain Size Larger than 15 microns

[[ ]]

Figure 1.10: Predicted/Measured FGR as a function of Exposure for Fuel Rods with Grain Size Larger than 15 microns

[[ ]]

Figure 1.11: Predicted minus Measured FGR as a function of Exposure for Fuel Rods with Grain Size Larger than 15 microns (measured FGR <5%)

[[ ]]

Figure 1.12: Predicted vs. Measured Diametral Strain for Fuel Rods with Grain Size Larger than 15 microns (Creepdown Data Only)

[[ ]]

Figure 1.13: Predicted minus Measured Diametral Strain vs. Expsosure for Fuel Rods with Grain Size Larger than 15 microns (Creepdown Data Only)

[[ ]]

Figure 1.14: Predicted vs. Measured Diametral Strain for Fuel Rods with Grain Size Larger than 15 microns (Ramp Tests Data Only)

[[ ]]

Figure 1.15: Predicted - Measured Diametral Strain vs. Expsosure for Fuel Rods with Grain Size Larger than 15 microns (Ramp Tests Data Only)

RAI-1.e (full text)
Please provide a plot showing LHGR vs. burnup for rods that PRIME has been compared to with each rod shown with a different symbol. Also discuss what experience you have with high burnup fuel under AOO and accident conditions (if the code is applied to a specific accident).

Response:

Local LHGR as a function of local exposure is shown in Figure 1.16 for all rods in the PRIME qualification database. To limit the number of data points in this plot, for each 5 GWd/MTU interval, one Peak LHGR was selected for each rod and plotted as a function of local exposure from the corresponding node for the same time step. Local LHGR vs. local exposure for PRIME FGR, fuel centerline temperature, and diametral strain qualification rods are shown in Figure 1.17 to 1.19, respectively. PRIME steady state results will be used to initialize the LOCA analyses. PRIME will not be applied to fast AOOs or RIAs until NRC approval of an addendum to the subject LTR. This supplement will discuss the available transient models in PRIME and their application to the fast AOOs and RIA analyses.

[[ ]]

Figure 1.16: Local LHGR vs. Local Exposure for all the Rods in PRIME Qualification Database

[[ ]]

Figure 1.17: Local LHGR vs. Local Exposure for PRIME FGR Qualification Rods (Rods designated with "Others" legend include all the rods with MLGR< 13 kW/ft and local exposure <75 GWd/MTU)

[[ ]]

Figure 1.18: Local LHGR vs. Local Exposure for PRIME Fuel Temperature Qualification Rods

[[ ]]

Figure 1.19: Local LHGR vs. Local Exposure for PRIME Diametral Strain Qualification Rods

RAI-1.f (full text)
This table does not specify the cladding type that PRIME should be limited to. Please list the cladding alloy(s) and type(s) (e.g. RXA or CW-SRA, etc.) that have sufficient qualification data and that the code may be applied to.

Response:

The code has an option to treat either RXA Zircaloy or CWSR Zircaloy. The RXA properties are based upon RXA Zr-2 data and the CWSR properties are based upon CWSR Zr-4 data. RXA Zr-2 cladding is used primarily for BWR fuel and CWSR Zr-4 cladding is used primarily for PWR fuel. The qualification includes both BWR and PWR data.

NEDC-33256P – Technical Basis

RAI-2 (full text)

Section 3.1 of NEDC-33256P describes the model that is used for crud conductivity. For a typical crud thickness of 0.5 mils this model gives a conductivity almost [[ ]] than is used by FRAPCON (~0.87 W/m-K). Please provide data to justify this model.

Response:

For BWR plants with normal water chemistry, the crud that forms on fuel rods is soft and fluffy and promotes 'wick' boiling. [[ ]]. In the LTR, the referenced model is Option 2. For instances where the referenced model is judged not applicable, such as in cases [[ ]] In this option, [[ ]]and an appropriate conductivity [[ ]]

RAI-2 Supplement 1 (full text)

A specific example is needed for each option along with values for Kcrud and Koxide along with how each crud and oxide thickness is determined for a specific plant application. Also, what criteria/guidelines determine which option is used?

Response:

[[ ]]and the nominal rate is specified as [[ ]] inches per year. The upper 2σ values used in statistical analyses are [[ ]] and [[ ]] inches per year, respectively. In both cases, the crud thermal conductivity is defined as

Kcrud = [[ ]]/THK

where

THK = crud thickness, inches
Kcrud = conductivity, BTU/hr-ft-oF

The PRIME model contains [[

]] For either option, the oxide thickness and conductivity are specified as discussed in the response to RAI-34 follow-up question.

NEDC-33256P – Technical Basis

RAI -03 (full text)

Section 3.1 of NEDC-33256P describes the model that is used for cladding conductivity. The model for zirconium conductivity under predicts data below 500K from *J.K. Fink and L. Leibowitz, J. Nuclear Materials, v226, p44 (1995) and C.Y. Ho, R.W. Powell and P.E. Liley, J. Phys. Chem. Ref. Data, v1, p279 (1972)*. Please provide data to justify this model.

Response:

As noted in Table 2.1 of NEDC-33256P the applicability range for cladding temperature is [[ ]]. In this range the PRIME zirconium conductivity model agrees well with the Reference 3.1 recommended model as shown in Figure 3.1. The slight differences in prediction at around 300 K are well within the 1 standard deviation of the Reference 3.1 model.

[[ ]]
Figure 3.1: Zirconium Conductivity Comparison

Reference:

[3.1] J.K. Fink and L. Leibowitz, "Thermal Conductivity of Zirconium", J. Nuclear Materials, v226, p44 (1995).

NEDC-33256P – Technical Basis

RAI-04 (full text)

Section 3.3.2 of NEDC-33256P discusses the radial power profile within UO2 but does not address the radial power profile for UO2-Gd2O3 fuel.

a. Please discuss how PRIME determines the radial power profile for UO2-Gd2O3 fuel along with an example of the values used for 5 and 10 wt% Gd2O3 concentrations.
b. Please provide an equation that demonstrates how the fission plus gamma heating are used to determine the normalized effective fission density used in the fuel temperature calculation.

Response

a. The impact of gadolinia was looked at several years ago. Because [[

]]During development of PRIME, a RPD based upon the [[

]] It was concluded that the RPD currently in the code provides the best fit to high burnup RPD data.

b. The referenced radial power distribution describes fission power distribution with the pellet, normalized to the pellet centerline fission density. The gamma heating is assumed to be uniform across the pellet and is input as a fraction of nuclear power due to gamma interaction [[ ]] Within the code the RPD is normalized to [[

]]

RAI-04 Supplement 01 (full text)

A specific example of this calculation is needed.

Response:

As indicated in the response, the referenced radial power distribution describes fission power distribution with the pellet, normalized to the pellet centerline fission density. The gamma heating is assumed to be uniform across the pellet and is input as a fraction of nuclear power due to gamma interaction [[ ]] Within the code the RPD is [[ ]] (typically at a normalized radius between [[ ]] to pellet average (nominal) power. [[

]]

An example of the calculation of the effective fission power density is shown in Figure 4.1 below for a GE14 pellet with 4% enrichment at 40 GWd/MTU and assumed gamma heating [[ ]]. The fission power distribution, obtained from the referenced radial power distribution is renormalized to 1.0, resulting in a value of[[ ]]. This distribution is combined with a uniform distribution of [[ ]] and again renormalized to 1.0 to obtain the effective radial power distribution. The effect of gamma heating is to flatten the effective distribution slightly relative to the fission power distribution.

[[ ]]
Figure 4.1: Fuel Pellet Radial Power Distribution

NEDC-33256P – Technical Basis

RAI-05 (full text)

Section 3.3.4 of NEDC-33256P describes the grain growth model and a description of how it was fit to data. Please provide some data comparisons to demonstrate how well this model predicts grain growth for UO_2 and UO_2-Gd_2O_3. Also, how will this model be applied for [[ ]]fuel?

Response:

Data comparison for the PRIME grain growth model is shown in Figure 5.1 to 5.4 for the UO_2 and UO_2-Gd_2O_3 rods. For the [[ ]]fuel the grain growth model for the UO_2 fuel will be applied.

[[ ]]

Figure 5.1: Predicted vs. Measured Grain Growth

[[ ]]

Figure 5.2: Predicted/Measured Grain Growth vs. Nodal Exposure

[[ ]]

Figure 5.3: Predicted/Measured Grain Growth vs. Initial Grain Size

[[ ]]

Figure 5.4: Predicted/Measured Grain Growth vs. Peak LHGR

RAI-5 (Supplement 1): Grain growth comparison to RISO-III GE ramp test fuel rods

Response:

RISO-III GE ramp test rods are summarized in Table 5-1. These cases are added to the existing PRIME grain growth qualification database and the new comparison is shown in Figure 5.5 to 5.8.

Table 5-1: RISO-III GE Ramp Test Rods

Rod ID	Axial Position (Node #)	Node Burnup (MWd/t)	Node Terminal Power (kW/ft)	Grain Size (micrometer)				Predicted / Measured (-)
				Initial (3D)	After ramp			
					Measured (2D)	Measured (3D)	Predicted (3D)	
[[								
								]]

[[ ]]

Figure 5.5: Predicted vs. Measured Grain Growth

[[ ]]

Figure 5.6: Predicted/Measured Grain Growth vs. Nodal Exposure

[[ ]]
Figure 5.7: Predicted/Measured Grain Growth vs. Initial Grain Size

[[ ]]
Figure 5.8: Predicted/Measured Grain Growth vs. Peak LHGR

NEDC-33256P – Technical Basis

RAI-06 (full text)

NEDC-33256P does not describe a model for oxide conductivity. The oxide conductivity is used in Equation 3-6. Please provide a description of the oxide conductivity model and the data used to justify this model.

Response:

The oxide thickness model is described in the response to RAI-34. The thermal conductivity used in conjunction with the input oxide thickness is [[ ]] Btu/hr-ft-^{o}F. This oxide conductivity value is based on measurements performed on GE fabricated fuel rods irradiated in commercial reactors. These measurements were made at a [[ ]] Follow-on experiments were performed to confirm the validity of this conductivity value at reactor operating temperature. It is noted that this value is consistent with the MATPRO (Reference 6.1) Zircaloy oxide correlation and data reported by Adams et. al. (Reference 6.2).

Reference:

[6.1] MATPRO -- A Library of Materials Properties for Light-Water-Reactor Accident Analysis, NUREG/CR-6150, Volume IV.

[6.2] M. Adams, “Thermal Conductivity: III, Prolate Spheroidal Envelope Method," Journal of the American Ceramic Society, 37, 1954, pp. 74-79.

NEDC-33256P – Technical Basis

RAI-07 (full text)

Please provide annealing data in terms of irradiated yield and ultimate tensile strength to support the model presented in Section 4.2 of NEDC-33256P.

Response:

During operation, Zircaloy cladding is subjected to fast neutron flux. The accumulated fast fluence hardens the Zircaloy. The irradiation hardening is subjected to concurrent thermal annealing. At normal operating temperatures, annealing effects are explicitly addressed in the steady-state hardening calculation. However, for analysis of AOOs, the effects of short term annealing must be adequately addressed to assure that the yield stress used to calculate cladding plastic strain during the AOO accurately or conservatively reflects the effects of annealing.

The cladding temperature during AOOs depends upon the specific AOO and the exposure at which it occurs, but a representative maximum cladding temperature for [[ ]]. At this temperature the relation for annealing time constant in the PRIME model results in a time constant of [[ ]] The duration of the AOO is assumed to be [[ ]]. Thus over [[ ]] of the irradiation hardening is annealed out. Reference 7-1 specifically addresses short term annealing of irradiation hardening in irradiated Zircaloy-2 barrier cladding. In general, the results indicate minimal annealing for [[ ]] Specifically, using the annealing relation developed in this reference, approximately [[ ]] of the irradiation hardening is annealed out. This result indicates that the PRIME treatment of annealing at AOO temperatures is conservative.

Reference:

[7-1] Torimaru, T., Yasuda, T. and Nakatsuka, M., "Changes in Mechanical Properties of Irradiated Zircaloy-2 Fuel Cladding due to Short Term Annealing," Journal of Nuclear Materials 238 (1996) 169-174.

RAI–07 Supplement 1 (full text)

Please confirm that the formulation for yield stress of CWSR Zircaloy as reported in the NEDC-33256P page 4-4 is correct.

Response:

At the request of PNNL, GNF has reviewed the formulation for yield stress of CWSR Zircaloy in the PRIME LTR. Based upon this review, GEH concludes that the formulation is incorrectly stated in the LTR. Specifically, on page 4-4, the saturation value of the fluence dependent term V in the relation for the strain hardening exponent n is [[ ]] The correct value is [[ ]] and will be incorporated in the –A version of PRIME LTR. The PRIME coding does not include this error. A plot of yield stress versus fluence for CWSR Zircaloy at 350°C is given below.

[[ ]]

RAI –07 Supplement 2 (full text)

Please provide the basis for the Zirconium yield stress.

Response:

GNF has performed tensile tests of irradiated zirconium sheets of two different purities. [[

]] Results of these tensile tests are shown in Table 1. These results were confirmed with the microhardness measurements on both the barrier and Zircaloy-2 portions of unirradiated and irradiated barrier tubing. Although not a direct measurement of yield stress, comparison of hardness provides a relative indication of yield stress. Results of the measurements are presented in Figure 1. These results indicate that the hardness of unirradiated zirconium is [[

]] These results are consistent with the expression for yield stress of zirconium and annealed Zircaloy given in Section 4.1.3 of NEDC-33256P.

Table 1: Tensile Tests of Zirconium Irradiated at 327°C to Fluence 6.8×10^{20} n/cm^2 (E>1 MeV)

Specimen	Tests	0.2% Offset Yield Strength (ksi)	Ultimate Strength (ksi)
Annealed Zirconium Sponge	Test 1	[[	
	Test 2		
Annealed Crystal Bar Zirconium	Test 1		
	Test 2		
	Test 3		]]

[[

]]

Figure 1: Knoop Microhardness vs. Fast Neutron Fluence for Zirconium and Zircaloy-2

NEDC-33256P – Technical Basis

RAI-08 (full text)

Section 5.1 of NEDC-33256P describes the model for cladding thermal expansion. The PRIME model appears to predict more thermal expansion than FRAPCON between 500 and 1000K by about 25%. Please provide thermal expansion data to justify the use of this model.

Response:

During the preparation of this RAI response, GNF noticed an error in the NEDC-33256P Section 5.1 (page 5-1 and 5-2) cladding thermal expansion model. The correlation for cladding thermal expansion coefficients as reported in equation 5-1, 5-2 and 5-3 are derived for the recrystallized annealed (**RA**) Zircaloy and Zirconium materials assuming typical tube texture [[ ]], respectively. However, the thermal expansion coefficient correlations for the cold worked stress relieved (**CWSR**) materials were mistakenly not included in the PRIME LTR. The thermal expansion of CWSR Zircaloy-2 and Zircaloy-4 tubing is given by the following expressions:

Longitudinal direction,

[[ ]]

Radial and circumferential direction

[[ ]]

where,

T = cladding average temperature (°F)

These thermal expansion coefficients for CWSR material will be included in the –A version of the PRIME LTR. Figure 8.1 and 8.2 show comparisons between PRIME cladding thermal expansion model for annealed and CWSR material in the longitudinal and circumferential direction, respectively. As shown in Figure 8.1 and 8.2, PRIME calculates [[ ]] thermal expansion for the annealed material than the CWSR material. Comparisons of PRIME models with the measured thermal expansion data (References 8.1 – 8.5) are also shown in Figures 8.1 and 8.2. The PRIME models generally agree well with these data. The differences between the PRIME and FRAPCON models can be attributed to the differences between the [[

]]

[[ ]]

Figure 8.1: Comparison of PRIME thermal expansion models (longitudinal direction) with measured thermal expansion data.

[[ ]]

Figure 8.2: Comparison of PRIME thermal expansion models (circumferential direction) with measured thermal expansion data.

The PRIME relations for cladding thermal expansion are obtained by [[

]] and comparing the results to available data. The comparisons for GNF RA Zircaloy-2 tubing are presented in Figures 8.1 and 8.2 of the revised response to RAI 8. In these figures, only the Mehan and Weisinger data is for Zircaloy-2, but the data was measured for plate specimens with unspecified texture. In the temperature range of interest for normal reactor operation, the difference between the PRIME results and the Mehan and Weisinger results are approximately [[ ]] in/in. Some of this difference, particularly in the circumferential direction, can be attributed to texture differences for tubing and plate. For example, if the PRIME results in the circumferential direction are recalculated using a typical transeverse texture factor for plate material, the results agree very closely with the Mehan and Weisinger data.

The impact of the differences noted above on results of PRIME licensing analyses are as follows. Not accounting for the possible texture impact noted above, the PRIME circumferential relation results in larger cladding diametral thermal expansion. The difference between the thermal expansion due to the PRIME relation and the data is [[ ]] This difference is small relative to the [[

]]. Similarly, the PRIME longitudinal relation results in [[ ]] The difference between the thermal expansion (over the entire length of the rod) due to the PRIME relation and the data is [[ ]] Again, this difference is small in terms of impact on rod void volume relative to the PRIME model uncertainty and uncertainties that impact rod void space addressed in the PRIME application methodology. The difference is also small relative to the total cladding length increase due to irradiation growth and thermal expansion at high burnup, where rod internal pressure is limiting.

References:

[8.1] L. R. Bunnell et al., High Temperature Properties of Zircaloy Oxygen Alloys, EPRI NP-524, March 1977.
[8.2] D. L. Douglass, "The Physical Metallurgy of Zirconium," Atomic Energy Review, 1, 4, December 1963, pp. 73-74.
[8.3] R. L. Mehan and F. W. Wiesinger, Mechanical Properties of Zircaloy-2, KAPL-2110, February 1961.
[8.4] P. B. Scott, Physical and Mechanical Properties of Zircaloy-2 and -4, WCAP-3269-41, May 1965.
[8.5] J. J. Kearns, Thermal Expansion and Preferred Orientation in Zircaloy, WAPD-TM-472, November 1965, pp. 17-18.

NEDC-33256P – Technical Basis

RAI-09 (full text)

Section 5.2 of NEDC-33256P on cladding irradiation growth states that this model is fit to an expanded database of LWR rod growth. Please provide a figure showing these data and the model predictions.

Response

Fuel rod axial growth occurs due to irradiation growth and stress induced creep.[[

]] The database is summarized in Figure 9.1.

[[

]]

Figure 9.1 Irradiation Growth of Zircaloy

RAI-09 Supplement 1 (full text)

Are their additional growth data above 10 E21 n/cm^2 because the data provided in this range is very limited?

Response:

The data provided was obtained from length change measurements of water rods, unfueled fuel rods, and specifically fabricated test specimens. A fluence of [[ ]] GNF is currently obtaining and processing channel length data inferred from bow measurements on bundles with exposures in the range of [[ ]] to expand the database for fluence above [[ ]]

RAI-9S02 (full text)
Provide more growth data (if available) above 10e21 n/cm2 fluence.

Response:
As noted in the original response to RAI-9, fuel rod axial growth occurs due to irradiation growth and stress induced creep. [[ ]]
As noted in the original response, GNF has continued to expand the irradiation growth database by inclusion of new high fluence growth data from water rods, channels, and other components with low axial stress during normal operation. The expanded database is shown in Figure 9.2. In this figure, data previously provided to the NRC are shown with the red triangle symbols. The other data is the new high fluence data. This data significantly expands the database for fluence above [[ ]]

[[ ]]

Figure 9.2: Irradiation Growth of Zircaloy (additional data)

NEDC-33256P – Technical Basis

RAI 10 (full text)

Please provide the data or a reference (if the data is publicly available) for the fuel swelling model derived in Section 5.3 of NEDC-33256P and a figure showing the PRIME model predictions to these data.

Response:

Fuel pellet swelling model/rate defined in section 5.3 of NEDC-33256P has been quantified by direct continuous on-line measurements of the fuel column length for two fuel rods irradiated in an experimental fuel assembly in the HBWR at Halden. Changes in the fuel column length were measured by a linear-variable-differential-transformer (LVDT) affixed to the fuel pellet column. One fuel rod contained pellets with a high matrix density and artificially induced porosity to achieve a [[ ]] TD overall pellet density. The second fuel rod contained high density [[ ]] pellets. The length change measurement results are shown in Figure 10.1. Based upon these measurements, a best estimate swelling rate of [[ ]] has been adopted.

[[ ]]
Figure 10.1: Fuel Column Length Change Measurements

This best estimate fuel pellet irradiation swelling rate has been confirmed at higher exposures by pellet density measurements taken on normal production fuel pellets irradiated in a commercial reactor. These density measurement results are presented in Figure 10.2 and confirm the applicability of the best estimate fuel irradiation swelling rate for both UO_2 and $(U, Gd)O_2$.

[[ ]]

Figure 10.2: Pellet Density Measurements

Recently, GNF/NUPEC collected high exposure pellet swelling data by measuring the density of the irradiated pellets. In three different programs, fuel pellet density after irradiation was measured for several cycles up to [[ ]] The measured density data are summarized in Figure 10.3. These data suggest a higher swelling rate above [[ ]]. The current PRIME model assumes a constant swelling rate of [[ ]] Based upon the very good PRIME predictions of cladding strain for exposure both below and above [[ ]] As shown in NEDC-33257P Section 3, cladding profilometry of GNF commercial rods confirm that PRIME cladding strain predictions at high exposure using this swelling rate agree well with measured strains.

[[ ]]

Figure 10.3: Measured Pellet Density Data from Three Different NUPEC Programs for 8x8 BWR Fuel.

NEDC-33256P – Technical Basis

RAI-11 (full text)

Section 5.4 of NEDC-33256P describes the fuel densification model. The model described in Equation 5-11 contains the parameter, "M" that does not have a value given. The text states that "M" is calculated using the maximum densification value. Please provide a description or a sample calculation that shows how M is calculated from the maximum densification value and how the maximum densification is determined for the different analysis applications.

Response:

The fuel densification model includes constants A and M. [[

]] For PRIME application, the densification model in Equation 5-11 is used to solve for M using the results of thermal resintering tests. [[

]]

NEDC-33256P – Technical Basis

RAI-12 (full text)

No hydrogen pickup model has been described in the document. Will PRIME be used to calculate cladding hydrogen content?

Response:

During the February 12-13, 2008 NRC/GNF meeting, GNF proposed a cladding hydrogen limit of [[ ]] The basis for the proposed limit is discussed in detail and documented in the Addendum to the Response to ESBWR RAI 4.2-2 and 4.2-4.

PRIME currently does not contain the capability to calculate hydrogen concentration, although such a calculation could be performed using the calculated oxide thickness, as discussed in the response to RAI-34, and a user input hydrogen pickup fraction. Rather, in conjunction with the proposed hydrogen limit, GNF proposed a model for cladding hydrogen concentration as a function of local burnup. This model will be used to confirm that the hydrogen concentration limit is satisfied for each PRIME application.

NEDC-33256P – Technical Basis

RAI-13 (full text)

A discussion is provided in Section 5.4 of NEDC-33256P about an option in PRIME to provide a different axial densification value that is different from that in the hoop and radial directions. Please provide a discussion on when and why this option is used and the code to data comparisons that justify the use of this option.

Response:

This option was provided in the GEPAP/TEXICO CODES when densification magnitude was larger to permit conservative calculations by biasing the densification in either the radial or axial direction. This option is not used for the PRIME code. Reference to these different axial densification values will be removed from the –A version of the PRIME LTR.

NEDC-33256P – Technical Basis

RAI-14 (full text)

Please provide cladding deformation data to support the fuel Poisson's ratio and fuel creep model assumptions for fuel with the proposed additives given in Section 5.7 of NEDC-33256P.

Response:

A separate LTR for additive fuel including the PRIME additive models will be submitted to the NRC for review and approval around [[ ]]. Following NRC approval of the additive LTR, PRIME will be used for the design and licensing of fuel containing the specified fuel additive.

NEDC-33256P – Technical Basis

RAI-15 (full text)

The algorithm for axial slip between the fuel and cladding when the gap is closed is not clear as defined in Section 5.9 and Figure 7.3 (b) of NEDC-33256P. Does this algorithm allow for complete lockup of the fuel and cladding, i.e., no axial slip between fuel and cladding? If so, it is not clear how complete lockup and the allowance of slip is determined when the gap is closed. Please provide an example with numerical values of how the axial cladding strain is determined due to axial fuel expansion when the gap is closed.

Response:

As LHGR increases in a rod, the fuel column and cladding expand independently in both the radial and axial directions. However, as the pellet-cladding gap closes, due either to relocation or pellet thermal expansion in the radial direction, differential axial expansion between the pellet and cladding results in build up of axial friction forces between the pellet and cladding. Axial locking can occur before hard radial contact between the fuel column and the cladding due to the fact that the fuel column is not a perfect right circular cylinder centered in a perfect right cylindrical tube.

The model was developed by calculating the elevation at which axial locking occurs in a fuel rod. [[

]] A typical result is shown schematically in Figure 15.1. [[

]] The components of the friction force are shown schematically in Figure 15.2a. [[

]] as shown in Figure 15.2b.

[[ ]]

Figure 15.1: Pellet Stacking in Loaded Fuel Rod

Notes:
Due to hourglassing look at pellet interfaces
[[

]]

[[ ]]
Figure 15.2a: Friction Force Components on Pellet i

Notes
[[

]]

[[ ]]
Figure 15.2b: Axial Loads on Pellet n

[[

]] The results are summarized in Figure 15.3. In Figure 15.3, the slip strain is given by

[[

]]

As shown in Figure 15.3, the slip strain increases with increasing diametral expansion until locking occurs.

[[ ]]
Figure 15.3: Axial Slip Strain versus Pellet Diametral Expansion Strain

Figure 15.3 shows that no axial strain is imposed by fuel column on the cladding until axial locking occurs. [[

]] As shown in Figure

15.3, the amount of pellet diametral expansion required for locking is [[
]]

The results in Figure 15.3 are presented differently in Figure 15.4. Figure 15.4 shows that the [[

]] The slip strain at locking is approximated by the relation

[[

]]

[[ ]]
Figure 15.4: Axial Slip Stain versus Axial Elevation

The values of S_1 and S_2 in the expression for maximum slip strain are determined by assuming that

[[ ]]

and determining the values of a, b and c to obtain the best fit to cladding diametral and axial strain data.

In summary, in PRIME, it is assumed that there is no axial interaction between the fuel column and cladding as long as the slip strain is less than maximum slip strain. [[

]]

NEDC-33256P – Technical Basis

RAI-16 (full text)

Please list the deformation data used to define the F_{comp} factor used for compliance of the rim in Section 6.1 of NEDC-33256P and show how this was determined from the data.

Response:

The Fcomp factor is determined using the high exposure (pellet average [[ ]]) diametral strain qualification data. First, the diametral strain qualification was performed assuming [[ ]]. Figures 16.1 and 16.2 show the results, which indicate that PRIME clearly [[

]]

To address these considerations, the PRIME diametral strain qualification was iterated by varying Fcomp [[ ]] This process yielded a value of [[ ]] The PRIME diametral strain qualification with [[ ]] is shown in Figure 16.3 and 16.4.

[[ ]]

Figure 16.1: Predicted vs. Measured Diametral Strain for [[ ]]

[[ ]]
Figure 16.2: Predicted - Measured Diametral Strain as a Function of Exposure for [[ ]]

[[ ]]
Figure 16.3: Predicted vs. Measured Diametral Strain for [[ ]]

[[ ]]

Figure 16.4: Predicted vs. Measured Diametral Strain as a Function of Exposure for [[ ]]

NEDC-33256P – Technical Basis

RAI-17 (full text)

Section 6.1 of NEDC-33256P explains how the precipitation of porosity (fission gas bubbles) due to rim formation is included in the fuel thermal conductivity of the rim. However, the precipitation of fission gas into bubbles reduces the matrix strain that results in an increase in the matrix thermal conductivity as demonstrated by Kinoshita et al (High Burnup Rim Project: (III) Properties of Rim-Structured Fuel, *Proceedings of the 2004 International Meeting on LWR Fuel Performance, Orlando, FL, September 19-22, 2004*). Does the rim thermal conductivity model in PRIME account for an increase in matrix conductivity due to precipitation of fission gas from the matrix? If so, show the combined impact on the rim conductivity as a function of burnup.

Response:

The PRIME rim thermal conductivity model [[
]].

RAI-17 Supplement 1 (full-text)

Provide details about the measured thermal diffusivity/ conductivity data that has been used to develop and verify the PRIME pellet thermal conductivity model.

Response:

The numerical thermal diffusivity data used to develop and validate the PRIME fuel pellet thermal conductivity model are provided in Reference 17.1. . Additional discussion about this database and the comparison to other open literature data are included in the response to RAI-20.

References:

[17.1] MFN09-106 Supplement 1, Data Package.

NEDC-33256P – Technical Basis

RAI-18 (full text)

Section 9 of NEDC-33256P provides a description of the calculation of void volumes and their associated temperatures. Please provide commercial fuel rod data that substantiates the value used for the stacking/chamfer volume, Vstack, in the rod internal pressure calculation. Please show the void volume due to the chamfer vs. Vstack at room temperature. Also please discuss how rs is calculated. If a Vstack value is used for validation of rod pressure from experimental rods please define how this value is determined. Please define any differences of approach between calculation of rod pressure for commercial rods and experimental rods.

Response:

In the PRIME model, for the calculation of hot (and cold) void volume, the contributions of initial pellet-cladding gap volume, initial plenum volume and initial dish volume and the evolution of these volumes with exposure are specifically included in the void volume calculation. Contributions not specifically included are addressed through the use of a 'stacking factor'. This factor quantifies the contributions of [[

]]

For each GNF fuel design, the stacking factor is determined from [[

]]

For application in the PRIME code, the stack factor is converted to a stack density. [[

]]

RAI-18 Supplement 1 (full text)

Discuss the contribution of pellet chamfer and enrichment marks in the void volume calculation.

Response:

The contribution of V_{stack} to the total void volume includes several contributions that can be summarized as follows:
[[

]]

[[

]] The respective contributions of these factors to V_{stack} break down as shown in the below table:

[[ ]]

Table 1

In this table, the ratio [[

]]

As shown in Table 1, for both the GE14 and GNF2 fuel designs, [[

]]

Some key nominal dimensions that can be used for such calculations are shown below:

[[ ]]

Table 2

[[

]] as represented by the equation:

[[

]]

The calculations performed to obtain the values in Table 1 are all based upon the nominal values listed in Table 2, with nominal enrichment marking area and depth as described below.

V_e, the volume of the enrichment marks, can also be calculated analytically.

]] For the purposes of the calculations in Table 1, the enrichment mark area is assumed to be [[

]] Figures 1 and 2 show photographs of the enrichment mark styles for GE-14 and GNF2 respectively, for clarification and comparison.

[[ ]]

Figure 1 – GE-14-Style Enrichment Mark

Figure 2 – GNF2-Style Enrichment Mark

[[

]]

NEDC-33257P – Qualification

RAI-19 (full text)

Section 2 of NEDC-33257P shows model to data comparisons of centerline temperature. Please provide additional comparisons to experimental rods that measured fuel centerline temperatures as discussed below.

a. *Some of the fuel temperature data comparisons from Halden used for code qualification in Sections 2.1 and 2.2 do not extend to the maximum burnup that these rods were irradiated to. IFA-432 Rods 2, 3, and 5 that were all irradiated to a rod average burnup above 30 GWd/MTU and data comparisons were only provided to 22 GWd/MTU. IFA-562 Rods 16, 17 and 18 were irradiated to a rod average burnup of more than 80 GWd/MTU and data comparisons were only provided to 57 GWd/MTU. Please make the comparisons to the IFA-432 (data provided in NUREG/CR-4717, note that elapsed time at power is incorrect and should be divided by 1.28 to get correct burnup values) and the IFA-562 (data provided in Halden report HWR-469) fuel temperature data up to the maximum burnup values provided in these reports.*

RAI – 19.a Supplement 1 (full-text)

Fuel Temperature predictions to data requested should include predicted/measured versus hot thermal gap and also versus gap conductance.

Combined Response (RAI-19.a & 19.a S01):

<u>IFA-432:</u>

The PRIME fuel temperature qualification database already included data up to [[
]] for IFA-432 rods 1, 2, and 3. Rod 4 was discharged early (at ~3 GWd/MTU) due to instrumentation failure. The PRIME temperature qualification database included reported data up to these burnups. For rod 5 the PRIME database included temperature data up to 22.9 GWd/MTU, although this rod had been irradiated up to 39.5 GWd/MTU according to the IFPE database. The PRIME qualification has been extended to the reported burnup for this rod and the qualification plots have been updated.

<u>IFA-562:</u>

As requested in the RAI, the fuel centerline temperature comparison has been extended for the IFA-562 rods 16, 17 and 18 based on the irradiation histories provided in Halden report HWR-469. A summary of additional qualification for IFA-432 and IFA-562 rods is provided in Table

19.1. The additional qualification is highlighted in the Table 19.1. The temperature qualification plots are shown in Figures 19.1-19.16.

Table 19.1: PRIME Fuel Temperature Qualification Database

Test Programs	Rods	PRIME Database (Corresponding to the NEDC-33257P) Local Burnup, GWd/MTU	Additional Qualification, Local Burnup, GWd/MTU
IFA-432	[[		
IFA-562			
			]]

[[ ]]

Figure 19.1: Predicted versus Measured Fuel Temperature for IFA-432 Rods 1-5

[[ ]]
Figure 19.2: Predicted/Measured Fuel Temperature versus Exposure for IFA-432 Rods 1-5

[[ ]]
Figure 19.3: Predicted/Measured Fuel Temperature versus Hot Mechanical Gap for IFA-432 Rods 1-5

[[ ]]

Figure 19.4: Predicted/Measured Fuel Temperature versus Hot Thermal Gap for IFA-432 Rods 1-5

[[ ]]

Figure 19.5: Predicted/Measured Fuel Temperature versus Hot Mechanical Gap for IFA-432 Rods 1-5 (Exposure<60GWd/MTU and Measured Temperature >1300°C only)

[[ ]]

Figure 19.6: Predicted/Measured Fuel Temperature versus Hot Thermal Gap for IFA-432 Rods 1-5 (Exposure<60GWd/MTU and Measured Temperature >1300°C only)

[[ ]]

Figure 19.7: Predicted/Measured Fuel Temperature versus Nodal LHGR for IFA-432 Rods 1-5

[[ ]]

Figure 19.8: Predicted/Measured Fuel Temperature versus Nodal LHGR for IFA-432 Rods 1-5 (Exposure<60GWd/MTU and Measured Temperature >1300°C only)

[[ ]]

Figure 19.9: Predicted/Measured Fuel Temperature versus Gap Conductance for IFA-432 Rods 1-5

[[ ]]

Figure 19.10: Predicted/Measured Fuel Temperature versus Gap Conductance for IFA-432 Rods 1-5 (Exposure<60GWd/MTU and Measured Temperature >1300°C only)

[[ ]]

Figure 19.11: Predicted versus Measured Fuel Temperature for IFA-562 Rods 15-18

[[ ]]

Figure 19.12: Predicted/Measured Fuel Temperature versus Exposure for IFA-562 Rods 15-18

[[ ]]

Figure 19.13: Predicted/Measured Fuel Temperature versus Hot Mechanical Gap for IFA-562 Rods 15-18

[[ ]]

Figure 19.14: Predicted/Measured Fuel Temperature versus Hot Thermal Gap for IFA-562 Rods 15-18

[[ ]]

Figure 19.15: Predicted/Measured Fuel Temperature versus Rod Average LHGR for IFA-562 Rods 15-18

[[ ]]

Figure 19.16: Predicted/Measured Fuel Temperature versus Gap Conductance for IFA-562 Rods 15-18

RAI-19.b (full text)

The code qualification data does not appear to include data from rods with fill gases other than helium. Because of this, it is difficult to determine if the code correctly accounts for the degradation in gap conductance and subsequent temperature increases when low conductivity fission gases are released when the gap is open. Please make comparisons to the following rods with low conductivity fill gases. IFA-432 Rod 4 (xenon fill gas), and IFA-633 Rods 1 (helium) and 2 (argon) for Ramp 1 (data provided in Halden report HWR-764). The comparisons to IFA-432 Rod 4 should include predicted minus measured versus burnup up to 10 GWd/MTU while the comparisons to IFA-633 Rods 1 and 2 (identical rods only fill gas is different) should provide measured versus predicted for Ramp 1.

RAI-19.b Supplement 1 (full text)

PNNL – A typo existed in the original RAI19, the request meant to compare to IFA-431 Rod 4, data provided in NUREG/CR-0318 and NUREG/CR-0797. Please plot measured temperatures versus burnup along with the predicted temperatures.

RAI-19.b Supplement 2 (full text)

Please provide predicted and measured centerline temperature versus local power for ramp 1.

Combined Response (RAI-19.b, RAI19.b S01 and RAI-19.b S02):

For IFA-633, fuel centerline temperature comparisons with PRIME predictions are shown for rods 1 and 3. Rod 1 was filled with Helium and rod 3 was filled with Argon. IFA-633 rod 2 is a MOX rod, which is [[ ]], and as a result [[ ]]. The additional comparisons for IFA-633 rods 1 and 3 are shown in Figures 19.17-19.22. Fuel temperature versus local burnup for IFA-431 rod 4 (Xe filled rod) is shown in Figure 19.23.

[[ ]]

Figure 19.17: Predicted versus Measured Fuel Temperature for IFA-633 Rods 1(Helium-filled) and 3 (Argon-filled) during Ramp 1

[[ ]]

Figure 19.18: Predicted/Measured Fuel Temperature versus Hot Mechanical Gap for IFA-633 Rods 1 and 3 during Ramp 1

[[ ]]

Figure 19.19: Predicted/Measured Fuel Temperature versus Hot Thermal Gap for IFA-633 Rods 1 and 3 during Ramp 1

[[ ]]

Figure 19.20: Predicted/Measured Fuel Temperature versus Gap Conductance for IFA-633 Rods 1 and 3 during Ramp 1

[[ ]]

Figure 19.21: Predicted/Measured Fuel Temperature versus LHGR for IFA-633 Rods 1and 3 during Ramp 1

[[ ]]
Figure 19.22: Fuel Temperature versus LHGR for IFA-633 Rods 1 and 3 during Ramp 1

[[ ]]
Figure 19.23: Fuel Temperature versus Local Burnup for IFA-431 Rod 4 (Xe flled rod)

RAI-19.c (full text)

The PRIME thermal conductivity model for UO2 results in significantly higher fuel thermal conductivity (> 10%) than that calculated using the Halden and FRAPCON-3.3 models at fuel temperatures between 800 °C and 2200 °C. Please provide a prediction of fuel centerline predictions and fission gas release for IFA-432 Rod 3 (small gap rod) and IFA-597.3 Rod 8 (data provided in Halden reports HWR-543 and HWR-599 and also in the IFPE database) providing comparisons to the measured data rod up to the maximum burnups where thermocouple measurements were made.

Response:
Fuel centerline temperature comparisons for IFA-432 rod 3 (small gap) and IFA-597 rod 8 are shown in Figure 19.24 to Figure19.27.

[[ ]]
Figure 19.24: Predicted versus Measured Fuel Temperature for IFA-432 Rod 3 and IFA-597.3 Rod 8

[[ ]]

Figure 19.25: Predicted versus Measured Fuel Temperature versus Exposure for IFA-432 Rod 3 and IFA-597.3 Rod 8

[[ ]]

Figure 19.26: Predicted/Measured Fuel Temperature versus Hot Thermal Gap for IFA-432 Rod 3 and IFA-597.3 Rod 8

[[ ]]

Figure 19.27: Predicted/Measured Fuel Temperature versus Gap Conductance for IFA-432 Rod 3 and IFA-597.3 Rod 8

RAI-19 remaining question (full text)

A table of predicted and measured centerline temperatures along with predicted fuel surface temperatures and gap conductance values for the above rods should be provided. Also, provide predicted/measured fuel temperatures versus burnup for all the rods with the exception of the IFA-633 rods. The IFA-633 fuel rods for Ramp 1 should provide predicted/measured versus linear power (LHGR) during the power ramp.

In order to determine if there is any bias in the predictions with respect to gap size or linear power, please provide predicted/measured fuel temperatures for all rods where PRIME fuel temperature predictions to data comparisons exist (including the above cases) versus predicted hot gap size and linear power (LHGR). Please identify in these figures those data with measured fuel centerline temperature above 1300°C at burnups up to 60 GWd/MTU and those above 1100°C for burnups above 60 GWd/MTU.

Response:

Tables of predicted and measured fuel centerline temperature along with predicted fuel surface temperature and gap conductance for the above rods are provided to NRC/PNNL in Reference 19.1. Figures 19.28 to 19.34 show the comparisons of PRIME predictions to measured fuel centerline temperature for the complete PRIME temperature qualification database.

[[ ]]

Figure 19.28: Predicted versus Measured Fuel Centerline Temperature for all PRIME Fuel Temperature Qualification Rods

[[ ]]

Figure 19.29: Predicted/Measured Fuel Centerline Temperature versus Exposure for all PRIME Fuel Temperature Qualification Rods

[[ ]]

Figure 19.30: Predicted/Measured Fuel Centerline Temperature versus LHGR for all PRIME Fuel Temperature Qualification Rods

[[ ]]

Figure 19.31: Predicted/Measured Fuel Centerline Temperature versus LHGR for all PRIME Fuel Temperature Qualification Rods (Blue Symbols: Exposure<60GWd/t and Measured Temperature >1300 ^{o}C and Red Symbols: Exposure>60GWd/t and Measured Temperature >1100 ^{o}C)

[[ ]]

Figure 19.32: Predicted/Measured Fuel Centerline Temperature versus Hot Thermal Gap for all PRIME Fuel Temperature Qualification Rods (Blue Symbols: Exposure<60GWd/t and Measured Temperature >1300 ^{o}C and Red Symbols: Exposure>60GWd/t and Measured Temperature >1100 ^{o}C)

[[ ]]

Figure 19.33: Predicted/Measured Fuel Centerline Temperature versus Hot Mechanical Gap for all PRIME Fuel Temperature Qualification Rods (Blue Symbols: Exposure<60GWd/t and Measured Temperature >1300 ^{o}C and Red Symbols: Exposure>60GWd/t and Measured Temperature >1100 ^{o}C)

[[ ]]

Figure 19.34: Predicted/Measured Fuel Centerline Temperature versus Gap Conductance for all PRIME Fuel Temperature Qualification Rods (Blue Symbols: Exposure<60GWd/t and Measured Temperature >1300 ^{o}C and Red Symbols: Exposure>60GWd/t and Measured Temperature >1100 ^{o}C)

Reference:

[19.1] MFN 09-106 Supplement 1, Data Package.

NEDC-33257P – Qualification

RAI-20 (full text)

It appears that the only centerline data comparison that has been made for UO2-Gd2O3 fuel is IFA 515.10 Rods A2 and B2. This fuel was made with non-neutron absorbing isotopes of gadolinium. In order to demonstrate the integral effect of the thermal conductivity, differing gadolinia wt%, and the radial power profile, please provide code to data comparisons for IFA-636 Rods 2 and 4 and IFA-681 Rods 2, 3, 4, and 6.

Response:

<u>IFA-636</u>

Halden irradiation experiment IFA-636 was performed to examine the behavior of gadolinia enriched fuel, subsequent to the IFA-515.10 test. The IFA-636 rig consists of 9 rods including 4 Gd (8wt%) rods. Among the Gd rods, only one rod (Rod 2) was equipped for fuel temperature measurement. Rod 4 had no thermocouple, but fuel temperature for this solid pellet fuel was evaluated from the measured temperature data for Rod 2 (hollow pellet fuel).

<u>IFA-681</u>

Halden irradiation experiment IFA-681 was also performed to examine the behavior of gadolinia enriched fuel, following the IFA-636 test. The IFA-681 test is in progress [[ ]]. Results for the 1st cycle of irradiation has been reported in a Halden report (HWR-815). The rig consists of 6 rods including two 2wt% Gd rods and two 8wt% Gd rods. For each concentration, one rod was a solid pellet rod with some hollow pellets to accommodate a thermocouple and one rod was a hollow pellet rod to accommodate an expansion thermometer. For the 2wt% Gd rods (Rod 2 and Rod 4), the linear heat rates reached about 11 kW/ft at about 3 GWd/MTU and saturated, indicating Gd burnout. For the 8wt% Gd rods (Rod 3 and Rod 8), the linear heat rate was about 5 kW/ft at about 2 GWd/MTU and was still increasing.

Predicted versus measured fuel centerline temperature for IFA-636 and IFA-681 rods are shown in Figure 20.1 and 20.2, respectively.

[[ ]]

Figure 20.1: Predicted versus Measured Fuel Centerline Temperature for IFA-636 Rods 2 and 4

[[ ]]

Figure 20.2: Predicted versus Measured Fuel Centerline Temperature for IFA-681 Rods

RAI-20 Supplement 1 (full text)

PRIME predicted fuel centerline temperatures for IFA-636 Rod 4 (with UO_2-Gd_2O_3) are significantly under predicted this data by 300F to 500F above 1800F while PRIME predicted the IFA-636 Rod 2 data well. The difference in these two rods is that the former is a solid pellet where the fuel temperature is estimated by Halden based on Rod 2 measurements while the latter is for an annular pellet with measured temperatures from a thermocouple placed in the annular pellet. The FRAPCON-3.3 code also predicts the Rod 2 measured temperatures well and under predicts Rod 4 but by a much smaller amount by 90F to 200F. The reason for PRIME under predicting Rod 4 by such a large amount needs to be explored further with the following requests.

A) Please provide the input used for Rods 2 and 4 as well a plot of the predicted and measured temperatures versus time. Also provide the gap conductance, hot thermal gap, and fuel surface temperature versus time.

B) Please provide the unirradiated and irradiated thermal conductivity data (based on thermal diffusivity measurements) used to develop and verify the UO_2-Gd_2O_3 conductivity model.

C) Also, please compare the PRIME thermal conductivity model for unirradiated UO_2-Gd_2O_3 to the data measured by Hirai et al. (Journal of Nuclear Science and Technology, vol. 28, issue 11, pp. 995-1000, 1991), Newman 1982 (DOE/ET/34212-36, 1982), Amaya et al. 1997 (Journal of Nuclear Materials, vol. 246, pp. 158-164, 1997). Compare PRIME model to the irradiated UO_2-Gd_2O_3 from Amaya et al. 2002 (Journal of Nuclear Materials, vol. 300, pp. 57-64, 2002).

General Comment:
In addition please compare to the unirradiated data from Ronchi et al (Journal of Applied Physics 85(2) pp.776-789, 1999) and to the irradiated data from Carrol et al. in Halden report HPR-345/13, 1994.

The comparisons to the IFA-681 rods appear to not be based on the latest available data in HWR-832 where the irradiation went to 340 days. At 340 days the 8wt% Rods 3 and 6 had their neutron absorbing Gadolinia burned out such that this comparison is particularly valuable. Please include the PRIME predictive comparisons to the fuel temperature data in this report.

Response:

Item A Response:

Inputs used for the PRIME analyses are summarized in Attachment 20-A. Fuel centerline and surface temperature comparisons for IFA-636 Rods 2 and 4 are shown in Figure 20.3 and 20.4, respectively. PRIME calculated hot thermal gap and gap conductance are shown in Figures 20.5 and 20.6, respectively.

[[ ]]

Figure 20.3: Fuel Centerline Temperature Comparisons for IFA-636 Rods 2 and 4

[[ ]]

Figure 20.4: Fuel Surface Temperature Comparisons for IFA-636 Rods 2 and 4

[[ ]]
Figure 20.5: Calculated Hot Thermal Gap versus Time for IFA-636 Rods 2 and 4

[[ ]]
Figure 20.6: Calculated Gap Conductance versus Time for IFA-636 Rods 2 and 4

Item B Response:

The PRIME thermal conductivity model is based on the laser flash diffusivity measurements on UO_2 and $(U,Gd)O_2$ fuel pellet samples and on fuel pellet samples fabricated to simulate the effects of exposure on thermal conductivity due to the accumulation of fission products. Comparison of the PRIME thermal conductivity model with the measured data both for the UO_2 and $(U,Gd)O_2$ rods are shown in Figure 20.7 to 20.9. The PRIME pellet thermal conductivity model agrees very well both for the UO_2 and $(U,Gd)O_2$ data without any specific bias with exposure or temperature.

[[ ]]

Figure 20.7: PRIME Pellet Thermal Conductivity Model Comparison

[[ ]]

Figure 20.8: Exposure Dependency of PRIME Pellet Thermal Conductivity Model

[[ ]]

Figure 20.9: Temperature Dependency of PRIME Pellet Thermal Conductivity Model

Item C Response:

Comparisons of the PRIME pellet thermal conductivity model with the literature data are shown in Figures 20.10 to 20.14.

[[ ]]

Figure 20.10: PRIME Pellet Thermal Conductivity Model Comparison with the data measured by Hirai et al. (Journal of Nuclear Science and Technology, vol. 28, issue 11, pp. 995-1000, 1991)

[[ ]]

Figure 20.11: PRIME Pellet Thermal Conductivity Model Comparison with the data measured by Newman 1982 (DOE/ET/34212-36, 1982)

[[ ]]

Figure 20.12: PRIME Pellet Thermal Conductivity Model Comparison with the data measured by Amaya et al. (Journal of Nuclear Materials, vol. 246, pp. 158-164, 1997)

[[ ]]

Figure 20.13: PRIME Pellet Thermal Conductivity Model Comparison with the data measured by Amaya et al. (Journal of Nuclear Materials, vol. 300, pp. 57-64, 2002)

[[ ]]

Figure 20.14: PRIME Pellet Thermal Conductivity Model Comparison with the data measured by Amaya et al. (Journal of Nuclear Materials, vol. 300, pp. 57-64, 2002)

Response to General Comments:

Comparisons of the PRIME thermal conductivity model with the Ronchi et al and Carrol et al. data are shown in Figures 20.15 and 20.16, respectively.

[[ ]]

Figure 20.15: PRIME Pellet Thermal Conductivity Model Comparison with the data measured by Ronchi et al (Journal of Applied Physics 85(2) pp.776-789, 1999)

[[ ]]

Figure 20.16: PRIME Pellet Thermal Conductivity Model Comparison with the data measured by Carrol et al. in Halden report HPR-345/13, 1994.

As requested, PRIME inputs were updated based on the HWR-832 report. Comparisons of the PRIME model with the measured data are shown in Figures 20.17 to 20.22.

[[ ]]

Figure 20.17: Predicted versus Measured Fuel Centerline Temperature for the IFA-681 Rods

[[ ]]

Figure 20.18: Predicted/Measured Fuel Centerline Temperature versus Rod Average Exposure for the IFA-681 Rods

[[ ]]

Figure 20.19: Predicted/Measured Fuel Centerline Temperature versus Hot Mechanical Gap for the IFA-681 Rods

[[ ]]

Figure 20.20: Predicted/Measured Fuel Centerline Temperature versus Hot Thermal Gap for the IFA-681 Rods

[[ ]]

Figure 20.21: Predicted/Measured Fuel Centerline Temperature versus LHGR for the IFA-681 Rods

[[ ]]

Figure 20.22: Predicted/Measured Fuel Centerline Temperature versus Gap Conductance for the IFA-681 Rods

RAI-20 Supplement 2 (full text)

Please provide more clarification about PRIME IFA-636 Calculations.

Response:

For IFA-636 Rod 2 and Rod 4, measured temperature data have been extracted from Halden reports HWR-723 Figure 11 and HWR-817 Figure 17, as shown in Figures 20.23 and 20.24, respectively. Comparisons of (calculated) PRIME fuel temperatures to measured temperatures for these rods are shown in Figure 20.25 and 20.26. PRIME predicts both the solid and hollow rods very well. For the initial PRIME calculations [[ ]]was assumed for these rods. If [[ ]]is assumed, the PRIME prediction for the solid pellet rod improves slightly relative to the estimated measured temperature for the solid pellet rod (Figure 20.26). The only differences between the PRIME predictions and the temperatures estimated by Halden for the solid pellet rod are observed between [[ ]]. These differences can be attributed to the uncertainty in the estimation technique used by Halden.

Also, for IFA-636 Rod 4, a difference was noted between the estimated measured temperatures used for the FRAPCON and PRIME comparisons. The estimated measured temperatures in Figure 20.27 (provided by PNNL) are consistently higher at low and high exposure than the HWR-817 Figure 17 reported temperatures. The differences between the PRIME and FRAPCON code predictions would be minimal relative to the measured data if results for both codes are compared with the HWR-817 Figure 17 reported data.

[[ ]]

Figure 20.23: IFA-636 Rod 2 Measured Peak Fuel Temperature (HWR-723 Figure 11)

[[ ]]

Figure 20.24: IFA-636 Rod 4 estimated Peak Fuel Temperature (HWR-817 Figure 17)

[[ ]]

Figure 20.25: PRIME comparison with IFA-636 Rod 2 (measured HWR-723 Figure 11)

[[ ]]

Figure 20.26: PRIME comparison with IFA-636 Rod 4 (estimated temp measurements: HWR-817 Figure 17)

[[ ]]
Figure 20.27: PRIME and FRAPCON comparisons with IFA-636 Rod 4 (as provided by PNNL)

RAI-20 Supplement 3 (full text)

Demonstrate with simple PRIME case that PRIME model adequately predict the fuel temperatures for a solid and hollow pellets.

Response:

For this evaluation a simple PRIME case has been constructed from the inputs provided for the PRIME RAI-38.a response. These inputs have been used for this demonstration since corresponding FRAPCON inputs are already available and can be easily modified for this demonstration. PRIME calculated fuel centerline temperatures for the solid and hollow pellets are compared at the beginning of life to be consistent with the simplified analytical solution presented in Attachment 20-C. For the PRIME calculation a [[ ]]is assumed for the hollow pellet case. For both cases, the LHGR is ramped from [[ ]]at zero exposure. The modified power history, together with the fuel design parameters used in these analyses, is shown in Attachment 20-B. Figure 20.28 shows that PRIME predicts about an [[ ]]for the solid vs. hollow pellet at about [[ ]], which is consistent with the analytical solution presented in Attachment 20-C.

[[ ]]

Figure 20.28: PRIME Calculated Fuel C/L Temperature versus LHGR for Solid and Hollow Pellets (results from Node 3 during the power ramp at zero exposure)

Attachment 20-A

PRIME Input Information for IFA-636 Rod 2 and Rod 4

Included in the Data Package (MFN09-106, Supplement 1)

Attachment 20-B

PRIME Input for the Simplified Analysis Case

Included in the Data Package (MFN09-106, Supplement 1)

Attachment 20-C

(Analytical solution for the hollow and solid pellet)

Steady State heat conduction equation in cylindrical coordinates

$$\frac{1}{r}\frac{d}{dr}\left(rk\frac{dT}{dr}\right)+Q=0$$ (Assumes uniform heat generation)

$$\frac{d}{dr}\left(rk\frac{dT}{dr}\right)+Qr=0$$

$$d\left(rk\frac{dT}{dr}\right)+Qrdr=0$$

Integrate

$$rk\frac{dT}{dr}+\frac{Qr^2}{2}+C_1=0$$

At $r=r_i$ $assume$ $\frac{dT}{dr}=0\rightarrow C_1=\frac{Qr_i^2}{2}$

$$rk\frac{dT}{dr}+Q\left(\frac{r^2}{2}-\frac{r_i^2}{2}\right)=0$$

$$K\ dT=-Q\left(\frac{r}{2}-\frac{r_i^2}{2r}\right)dr$$

Integrate $$\int_{Tc}^{Ts} KdT = -Q\left(\frac{r^2}{4} - \frac{r_i^2}{2}\,lnr\right)\Bigg|_{r_i}^{r_o}$$

$$Q = 1087\,\frac{LHGR}{r_0^{\,2} - r_i^{\,2}}$$

Then $$\int_{Ts}^{Tc} KdT = \frac{1087\,LHGR}{r_0^{\,2} - r_i^{\,2}}\left(\frac{r^2}{4} - \frac{r_i^2}{2}\,lnr\right)\Bigg|_{r_i}^{r_0}$$

For $r_i = xr_0$

$$\int_{Ts}^{Tc} KdT = \frac{1087\,LHGR}{\left(1 - X^2\right)r_0^{\,2}}\left(\frac{r_0^{\,2}}{4} - \frac{x^2 r_0^2}{2}\,In\,r_0 - \frac{x^2 r_0^2}{4} + \frac{x^2 r_0^2}{2}\,ln\left(xr_0\right)\right)$$

$$= \frac{1087\,LHGR}{\left(1 - X^2\right)}\left(\frac{1 - x^2}{4} + \frac{x^2}{2}\,ln\,X\right)$$

[[ ]]

For $X = 0$

[[ ]]

For $X \neq 0$

[[ ]]

Ratio of [[ ]]

$$X \quad \frac{I_{Hollow}}{I_s}$$

[[

]]

The relations above will be used to compare PRIME temperature predictions for solid and hollow pellets. To permit analytic integration of K with respect to T it is assumed that

Bu = 0

Gd = 0

Then for [[ ]]

[[ ]]

Where [[ ]]

$$T = F$$

Then

[[ ]]

And

[[

]]

PRIME Results

UO2 Pellets
97% TD
BOL

	Solid X=0			Hollow [[ ]]				
LHGR (kW/ft)	Tc (oF)	Ts (oF)	I_s	Tc (oF)	Ts (oF)	I_{hollow}	ΔT* (oF)	(I_{hollow}/I_s)**
[[								
								]]

[[
]]

PRIME predicts impact of hollow pellets correctly over LHGR range

NEDC-33257P – Qualification

RAI-21 (full text)

The plots in Section 3 of NEDC-33257P show diametral strain from power ramp tests (PCMI) and from steady state irradiation (creepdown). Please provide plots of predicted diametral strain versus measured and predicted minus measured strain versus burnup only for low burnup rods where creepdown was present. Please provide the same plots for steady-state operation but at high burnups when the fuel-clad gap is closed and include cladding axial strain comparisons in addition to diametral strains. Please provide predicted versus measured and predicted-minus-measured versus terminal ramp power for the power ramped diametral and axial strain data. Provide these same comparisons for power ramped data but versus grain size and fuel additive content, respectively. Please discuss the possible reasons for the significant over prediction of diametral strains for three rods in Figures 3.1 and 3.2 and the over prediction axial strain of the four rods in Figures 3.3 and 3.4. Please provide a plot of ramped terminal power versus burnup that will demonstrate the breadth of the deformation database for AOOs.

Response:

Predicted versus measured diametral strain and predicted minus diametral measured strain versus local burnup for low burnup rods where creepdown was present are shown in Figures 21.1 and 21.2, respectively. Similar plots for high burnup when the fuel-clad gap has closed are shown in Figures 21.3 and 21.4. Figure 21.5 shows the predicted versus measured axial strain comparison for the high burnup rods. It is noted that PRIME significantly [[
]], as shown in Figures 21.3 and 21.5, respectively. [[
]]to demonstrate the consequence of operation of fuel with limited centerline melting. The irradiation histories for these rods are shown in Figure 21.6. PRIME calculations of the maximum fuel temperature for these significantly overestimated strain cases, together with calculated maximum fuel temperatures for the companion rods, are shown in Figure 21.7. It is likely that PRIME overpredicts the fuel temperature since these rods were operated with fuel melting (See Figure 21.8) and the PRIME calculation conservatively assumed [[
]]. As a result of this overestimation of fuel temperature [[
]] and, as a consequence, the cladding strain for these rods. The breadth of the PRIME cladding deformation database for AOOs is shown in Figures 21.9-21.14.

[[ ]]

Figure 21.1: Predicted vs. Measured Diametral Strain (Exposure < 30 GWd/MTU and Measured diametral strain < 0)

[[ ]]

Figure 21.2: Predicted minus Measured Diametral Strain vs. Local Exposure (Exposure < 30 GWd/MTU and Measured diametral strain < 0)

[[ ]]

Figure 21.3: Predicted versus Measured Diametral Strain (Exposure >40 GWd/MTU)

[[ ]]

Figure 21.4: Predicted minus Measured Diametral Strain vs Local Exposure (Exposure >40 GWd/MTU)

[[ ]]

Figure 21.5: Predicted versus Measured Axial Strain (Exposure >40 GWd/MTU)

[[ ]]

Figure 21.6: Irradiation histories for the 3 rods with significantly overpredicted strains

[[ ]]

Figure 21.7: PRIME Predicted Fuel Centerline Temperature of the Test Reactor Rods

[[ ]]

Figure 21.8: PRIME Predicted Fuel Melting Radius of the Test Reactor Rods

[[ ]]

Figure 21.9: Ramp Terminal Power versus Local Exposure for the PRIME Ramp Test Database

[[ ]]

Figure 21.10: Predicted versus Measured Diametral Strain for the PRIME Ramp Test Database Rods

[[ ]]

Figure 21.11: Predicted minus Measured Diametral Strain versus Ramp Terminal Power for the PRIME Ramp Test Database Rods

[[ ]]

Figure 21.12: Predicted minus Measured Axial Strain versus Ramp Terminal Power for the PRIME Ramp Test Database Rods

[[ ]]

Figure 21.13: Predicted minus Measured Diametral Strain versus Grain Size for the PRIME Ramp Test Database Rods

[[ ]]

Figure 21.14: Predicted minus Measured Axial Strain versus Grain Size for the PRIME Ramp Test Database Rods

NEDC-33257P – Qualification

RAI- 21 Supplement 1 (full text)

Provide PRIME calculated cladding profilometry comparisons for the GNF2 LUA rods inspected after 1st and 2nd cycle of irradiation at the KKM nuclear power reactor at Switzerland.

Response:

Four GNF2 fuel assemblies began operation in September 2005 as part of an LUA program at the KKM plant. The LUA fuel assemblies are currently in their third cycle of operation and are expected to reach [[ ]] bundle average exposure by the end of Cycle 35 (August 2008). As part of the LUA program, GNF has performed poolside visual examination of the bundle components, and COINS/profilometry measurements of selected fuel rods to assess fuel performance.

Two separate bundles were inspected after each of the first two operating cycles. Bundle JLL936, inspected after the first cycle of operation, reached an average bundle exposure of [[ ]]. Bundle JLL935, inspected after two cycles of operation, reached an average bundle exposure of [[ ]]. COINS and profilometry measurements have been analyzed to estimate the cladding diametral strain for direct comparison to PRIME03. The power and exposure histories for these fuel bundles were calculated using the nuclear accounting code PANACEA v11, which models the fuel assembly in ~6 inch axial nodes. This nodal power and exposure history was used as input to PRIME03.

For the purpose of defining the measured cladding diametral deformation, the average cladding diameter at each axial node is defined as:

[[

]]

This is compared to the predicted diameter, calculated using PRIME03 as:

[[

]]

The KKM GNF2 LUAs have been examined after both their 1st and 2nd cycle of operation. The rods selected for inspection were jointly determined by the Utility and GNF. Selection of candidate rods for poolside measurements are based on providing a reasonable spectrum of operation conditions to validate fuel design elements. Considerations include such factors as fuel exposure, peak nodal power, rod location within the lattice and relative to the blade and water channel, pellet enrichment, gadolina content, and lattice configuration as well as other factors. Figure 21.15 identifies the fuel rods inspected following cycle 33 and cycle 34. During the 1st fuel inspection, rod selection purposefully excluded partial length rods and tie rods due to fuel inspection equipment limitations. Given these constraints[[

]] Rod selection included rods [[

]] During the 2nd fuel inspection campaign, [[

]]

All rods measured during both inspection campaigns have been evaluated using PRIME03 to compare measured diametral change vs. predicted diametral change. The rods shown below have been provided to the NRC as representative results from this comparison.

1st Cycle Bundle JLL936
[[

]]

2nd Cycle Bundle JLL935
[[

]]

[[

]]

[[

]]

Figure 21.15: Location and exposures of rods selected for inspection

Figures 21.16 and 21.17 provide a comparison between the predicted fuel cladding OD and the measured fuel cladding OD of representative fuel rods after one cycle of operation in bundle JLL936 and two cycles of operation for bundle JLL935, respectively. The vertical bars shown on the measured data points in Figures 21.16 and 21.17 are the 95% confidence interval given the measurement variation observed [[ ]]
The vertical bars shown on the figures do not include variation associated with the COINS or profilometry measurement system, such as calibration variation and/or reproducibility, which are considered accurate to [[ ]], nor does it include assumption deviations for the tube OD used in the analysis. In the analysis, the tube OD is assumed a constant diameter once the reference has been established; in PRIME03, the reference is the nominal diameter (0.404 inch), and the calculated measured OD reference is based on the plenum diameter. Typical as-manufactured tube OD variation, which includes tube ovality and diameter variation, may deviate from the reference assumptions by [[ ]]. Cumulatively, these sources of variation, which are not included in the comparison, represent [[ ]] accuracy on the fuel cladding diameter, which is additive to the measurement variation and is consistent with the observation that the prediction may slightly over-predict or under-predict any specific rod.

As shown in Figure 21.16 and 21.17, GNF2 fuel rod diametral deformation after two cycles of operation to [[ ]] bundle average exposure compares well to the predicted fuel rod diameter using PRIME03. The minor differences between the measured and predicted diameters are well within both the uncertainty of the measurements and the differences in the reference nominal diameter used in the PRIME and measurement calculations.

[[ ]]
Figure 21.16(a): PRIME comparison with the GNF2 rod after 1st cycle of irradiation at the KKM power reactor (Bundle JLL936 Rod A8, [[ ]])

[[ ]]
Figure 21.16(b): PRIME comparison with the GNF2 rod after 1st cycle of irradiation at the KKM power reactor (Bundle JLL936 Rod J3, [[ ]])

[[ ]]
Figure 21.17(a): PRIME comparison with the GNF2 rod after 2nd cycle of irradiation at the KKM power reactor (Bundle JLL935 Rod G1, [[ ]])

[[ ]]

Figure 21.17(b): PRIME comparison with the GNF2 rod after 2nd cycle of irradiation at the KKM power reactor (Bundle JLL935 Rod H9, [[ ]])

NEDC-33257P – Qualification

NRC RAI 22

Please provide those data (predicted versus measured and predicted/measured versus burnup) used to develop and verify the cladding creep model and its uncertainty. If the IFA-585 creep experimental creep data for RXA Zry-2 (actual GE irradiated tubing from a commercial plant) were not used for verification, please compare to these data.

GNF Response

Figure 22.1 shows comparison of the PRIME low stress recrystallized Zircaloy and Zirconium creep relation with the data obtained by direct hoop strain measurements of pressurized cladding tubes irradiated in a commercial reactor. This creepout data was obtained [[

]] As shown in Figure 22.1, the PRIME correlation fits this data very well. Figures 22.2 to 22.4 show comparisons of the PRIME creep relation with open literature data. The data of the Halden creep experiment for recrystallized annealed Zicaloy-2 (IFA-585) were not directly used to develop the PRIME creep model. However, comparison of the PRIME creep relation with this data is shown in Figure 22.5. It is noted that only the [[

]]. As these materials were base irradiated for a long time before the creep tests, the primary creep contributions are not included in the PRIME calculations. Also, for the cladding liftoff calculation, one of the key applications of the PRIME creep model, [[

]]. This is an additional reason why only the steady state creep is compared with the Halden data. Figures 22.6 and 22.7 show the calculated versus measured and calculated minus measured versus time for all the data including IFA-585 data, respectively. It is noted that [[ ]] the overall agreement between the PRIME creep model and the data is very good. Based on these comparisons, the PRIME creep correlation uncertainty for the low stress creep region is [[

]].

[[ ]]

Figure 22.1: Comparison of PRIME creep relation with the Commercial Reactor Data

[[ ]]

Figure 22.2: Comparison of PRIME creep relation with the Ficara et. al.[22.1] Data

[[ ]]

Figure 22.3: Comparison of PRIME creep relation with the Rieger and Blood [22.2] Data

[[ ]]

Figure 22.4: Comparison of PRIME creep relation with the Babcock & Wilcox [22.3] Data

[[ ]]

Figure 22.5: Comparison of PRIME creep relation with the IFA-585 RXA Zr-2 data[22-4]

[[ ]]

Figure 22.6: Calculated vs. Measured Strain

[[ ]]
Figure 22.7: Calculated minus Measured Strain vs. Time

References:

[22.1] Ficara, PL et al., "Zircaloy-2 In-Pile Creep; Predicted-Measured Values Comparison", Enlarged Halden Program Meeting, Loen, Norway, June 1978.

[22.2] Rieger , GF and RE Blood, RE, "Creep of Zirconium alloys irradiated in the Big Rock Point BWR", CME Transmittal No. 78-212-0009, Rev. 1, February 27, 1978.

[22.3] "Hot Cell Examination of Creep Collapse and Irradiation Growth Specimens, End of Cycle 2" RP-711-1 EPRI/1 B and W Cooperative Program. Key Phase Report. No. 4, August 1979. LRC 4733-7, Babcock and Wilcox.

[22.4] M.A. McGrath, "In-Reactor Creep Behaviour of Zircaloy Cladding", ANS Int. Topical. Mtg. Light Water Reactor Fuel Performance, Park City, Utah, April 10-13 (2000).

NEDC-33257P – Qualification

NRC RAI 23

The data comparisons shown in Section 5 of NEDC-33257P on fuel rod internal pressure come entirely from test rods. Please include fuel rod internal pressure data comparisons from irradiated commercial rods, similar to the rods that PRIME will be applied to. If rod pressure data are not available please provide a comparison of void volume data from irradiated commercial rods versus PRIME predictions and also predicted/measured versus burnup.

GNF Response

Commercial rod data in the PRIME rod internal pressure qualification database is identified by solid red symbols in Figure 23.1 and 23.2. This dataset includes data from [[ ]] irradiated in commercial reactors. These rods were taken to hotcells and punctured to measure rod internal pressure at the end of irradiation. As shown in Figure 23.1 and 23.2, PRIME predicts this commercial rod data very well (as well or better than the test reactor data), particularly at high exposure.

[[ ]]

Figure 23.1: Predicted vs. Measured Rod Internal Pressure (red symbol: commercial rods data)

[[ ]]

Figure 23.2: Predicted - Measured Rod Internal Pressure vs. Exposure (red symbol: commercial rods data)

NEDC-33257P – Qualification

NRC RAI 24

PNNL does not have the capability to model UO_2 with Al_2O_3-SiO_2 additives in FRAPCON-3 and does not have access to a large database of properties for this fuel. Please provide model to data comparisons for UO_2 with Al_2O_3-SiO_2 up to the requested 2 wt% limit for the following models

a. Fuel thermal conductivity
b. Fuel thermal expansion
c. Fuel melting
d. Fuel temperatures
e. Fuel creep
f. PCI – Ramp test data

GNF Response

A separate LTR for additive fuel including descriptions of PRIME material properties for additive fuel will be submitted to the NRC for review and approval. Following approval of the LTR for additive fuel, PRIME will be used to design and license fuel containing the specified additive.

NEDC-33257P – Qualification

NRC RAI 25

The plots in Section 5 of NEDC-33257P show all of the FGR model to data comparisons on one plot. In order to determine the adequacy of the FGR model in PRIME, PNNL would like to see model to data comparisons for various subsets of the database in the range of application important to licensing analyses. Please provide the following comparisons to data with measured release values greater than 5% FGR absolute:

a. Plot predicted/measured versus burnup (separate steady-state and power ramped data).

b. For ramped rods, plot predicted/measured versus ramp terminal power level.

c. For ramped rods, plot predicted/measured versus ramp hold time at power.

d. Plot predicted/measured versus grain size (separate steady-state and power ramped data).

e. Please compare to the REGATE experimental ramped rod with a hold time of 1.5 hours in the IFPE database.

Response:

Predicted/measured fission gas release (>5%) data for steady state operation and power ramped data are plotted in Figure 25.1. Figure 25.2 and 25.3 show the predicted/measured FGR data for the power ramped rods versus ramp terminal power and hold time. Predicted/Measured FGR versus Pellet Initial Grain Size (FGR >5%) are shown in Figure 25.4, which also includes the REGATE rod with a hold time of 1.5 hours. GNF extracted the REGATE data from the IFPE database. This database doesn't include any information indicating whether the reported grain sizes are 2D or 3D. For plotting and PRIME calculations the reported grain sizes are assumed to be 3D grain sizes.

[[ ]]

Figure 25.1: Predicted/Measured FGR (FGR >5%) versus Rod Average Exposure

[[ ]]

Figure 25.2: Predicted/Measured FGR (FGR >5%) versus Ramp Terminal Power

[[ ]]

Figure 25.3: Predicted/Measured FGR versus Ramp Hold Time at Power.

[[ ]]

Figure 25.4: Predicted/Measured FGR versus Pellet Initial Grain Size (FGR >5%)

NEDC-33257P – Qualification

RAI-26 (full text)

It appears that the fission gas release (FGR) model in PRIME is the same for UO_2, UO_2-Gd_2O_3, and UO_2- Al_2O_3-SiO_2. In order to validate the model for these three fuel types, please provide the following figures

a. Predicted vs. measured FGR with each fuel type identified by a separate symbol
b. Predicted minus measured FGR for UO_2-Gd_2O_3 as a function of wt% Gd_2O_3.
c. Predicted minus measured FGR for UO_2- Al_2O_3-SiO_2 as a function of wt% Al_2O_3-SiO_2 distinguishing between different ratios of alumina-to-silicate.
d. Please provide predicted FGR, measured FGR, burnup, Gd_2O_3 or Al_2O_3-SiO_2 concentration, fuel grain size, experimental program, and ramp terminal power and hold time (for power ramped cases) in a table for each of the FGR assessment cases.
e. The fission gas release and cladding deformation data from the RISO3 program are not included in the fission gas release and deformation qualification databases. Please provide the data comparisons for the GE rods in this program. Also include tabulated fission gas release predictions for other rods that have been requested in these RAIs.

Response 26.a:

Predicted vs. measured FGR, with each fuel type identified by a separate symbol, is shown in Figure 26.1.

Response 26.b:

Predicted minus measured FGR for UO_2-Gd_2O_3 as a function of wt% Gd_2O_3 is shown in Figure 26.2.

Response 26.c:

A separate LTR with PRIME additive models and qualification will be submitted to the NRC for review and approval. Thus no further response is provided for this question.

[[ ]]
Figure 26.1: Predicted vs. measured FGR

[[ ]]
Figure 26.2: Predicted minus measured FGR for UO_2-Gd_2O_3 as a function of wt% Gd_2O_3.

RAI 26.d Response:

Predicted and measured FGR, burnup, Gd_2O_3 or Al_2O_3-SiO_2 concentration, fuel grain size, experimental program, and ramp terminal power and hold time (for power ramped cases) for the PRIME FGR qualification cases are summarized in tabular form in the attached data package (MFN 09-106 Supplement 1).

RAI 26.d (follow-up question)
We agree that the IFPE database does not specify 2D vs. 3D. We have a question to the IFPE database administrator about this, although PNNL's experience is if the grain size is not specified as 3-D the value is usually 2-D. Previous vendors that have compared to this rod assumed that the values provided were a 2-D grain size. Please re-examine the grain sizes for the RISO-1 data provided in the table for RAI-26.d because they appear to be 2-D based on report RISO-FGP-R10 Section 3.1 rather than a 3-D grain size. If the 2-D grain size values were used for PRIME predictions would these predictions change if 3-D values were used in the code and, if so, please provide the new predictions based on the 3-D values.

Response:
RISO-1 cases have been rerun assuming the reported grain size as 2-D. PRIME predictions for these rods are provided in the following Table.

Cases	Rod Avg. Expo, MWd/MTU	Measured FGR, %	PRIME Input grain size, microns (assuming the reported grain size is 3D)	PRIME FGR, % (assuming the reported grain size is 3D)	Revised PRIME Input grain size, microns (assuming the reported grain size is 2D)	PRIME FGR, % (assuming the reported grain size is 2D)
RISO1_IFA148_F14	[[					
RISO1_IFA148_F7						
RISO1_IFA148_F8						
RISO1_IFA148_F9						
RISO1_IFA148_G3						
RISO1_IFA148_G32						
RISO1_IFA148_G7						
RISO1_IFA148_J7						
RISO1_IFA148_M1						
RISO1_IFA148_M33						
RISO1_IFA148_M39						
RISO1_IFA148_M61						]]

RAI 26.e Response:

Cladding deformation and fission gas release for the RISO-III GE ramp tested rods are compared with PRIME calculations in Table 26.1 and 26.2, respectively. GE supplied GE2, GE4, GE6, GE7, II2 and II3 rods for this RISO-III ramp tests. As the [[
]], it is not included in the comparison. These rods are also included in the PRIME qualification database for fuel temperature and rod internal pressure. A table summarizing FGR predictions for rods in the RISO-I program is included in the RAI-26.d response.

Table 26.1: RISO-III GE Rods (Cladding Deformation Comparison)
[[

]]

Table 26.2: RISO-III GE Rods (Fission Gas Release Comparison)
[[

]]

NEDC-33257P – Qualification

RAI-27 (full text)
The qualification database for rod deformations and fission gas release includes data from PWR rods. Please explain how the PRIME deformation analyses of these rods were performed, particularly if the creep models in PRIME were not applicable to PWR cladding.

Response:

The PRIME code includes a creep model for cold-worked Zircaloy that is applicable to PWR cold-worked Zry-4 cladding. The code also includes different models from those for annealed or recrystalized Zircaloy for cold-worked Zircaloy cladding for irradiation growth and yield stress (< 450 deg C). Other models for cladding material responses and properties (such as thermal expansion, elastic modulus, irradiation hardening) are common for annealed and cold-worked Zircaloys. The cladding material type can be selected by a PRIME code input option.

The specific PRIME models for cold worked cladding are described in the following subsections of the PRIME LTR:

- Irradiation growth (section 5.2 of NEDC-33256P)
- Creep (section 5.6 of NEDC-33256P)
- Yield stress (strength coefficient) at low temperatures (section 4.1.3 of NEDC-33256P)

The code uses common models for cold-worked and annealed Zircaloy for the following cladding material responses and properties:

- Thermal expansion (section 5.1 of NEDC-33256P)
- Elastic Modulus (section 4.1.1 of NEDC-33256P)
- Poisson's ratio (section 4.1.2 of NEDC-33256P)
- Yield stress (strength coefficient) at high temperatures (section 4.1.3 of NEDC-33256P)
- Irradiation hardening and its recovery (section 4.1.3 and 4.2 of NEDC-33256P)

PWR rods with cold-worked Zircaloy cladding in the PRIME qualification database include the following:

- IFA-429 for temperature (2 rods) and for internal pressure (3 rods)
- RISO3 ANF rods for temperature (3 rods) and for internal pressure (4 rods)
- BR-3 for deformation qualification (5 rods)

NEDC-33257P – Qualification

RAI-28 (full text)

There appears to be a 40% variability in the calculated helium release. Please provide justification for why this uncertainty is not included in the rod pressure calculation. What is the effect of this uncertainty on a typical rod internal pressure calculation?

Response:

The reasons for not including the calculated helium release uncertainty in the rod internal pressure statistical evaluations are as follows:

- The amount of released helium is about one order smaller than the amount of released FP gases (Xe + Kr) for typical commercial fuel rods at high burnup, as shown in Figure 28.1 below. [[
]]

- [[

]] as shown in section 3.2.4 of NEDC-33258P. As shown in Figure 3-7 of NEDC-33258P (also shown here as Figure 28.2), [[

]]

[[ ]]

Figure 28.1: He Release/Fission Gas Release versus Rod Average Burnup

[[ ]]

Figure 28.2: Predicted vs. Measured Rod Internal Pressure with 2-sigma Model Perturbation

NEDC-33257P – Qualification

RAI-29 (full text)

Please tabulate the as-fabricated and measured post-irradiation grain sizes for the rods shown in Section 7 of NEDC-33257P. Identifying rod average burnup and whether the rods were steady-state or power ramped rods including the terminal ramped powers and hold times. Also identify if these grain sizes are MLI or 3D and how you convert between MLI grain size and 3D grain size.

Response:

The PRIME03 grain growth qualification database for power ramped rods and steady state operation rods are summarized in Table 29.1 and 29.2, respectively. The grain sizes listed in the tables are all 3D grain sizes. Grain sizes were measured by the intercept method and converted to 3D grain size by multiplying by 1.56.

Table 29.1: PRIME03 Grain Growth Qualification Database (Power Ramped Rods)
[[

]]

Table 29.2: PRIME03 Grain Growth Qualification Database (Steady State Operation Rods)
[[

]]

NEDC-33258P – Application Methodology

RAI-30 (full text)

Section 1.4 of NEDC-33258P describes a multi-node analysis and a 1-node analysis. Please provide a description of how a 1-node analysis is performed.

Response:

In the PRIME application methodology, a multi-node [[

]]

NEDC-33258P – Application Methodology

RAI-31 (full text)

The last sentence of Section 3.2.4.3 of NEDC-33258P suggests that a 2σ power uncertainty is applied for licensing analyses, please identify those models and analyses in which this uncertainty will be applied and how this will be applied.

Response:

For statistical analyses, [[

]] The results of the perturbation analyses are used to determine the combined uncertainty of the response parameter to the model and input parameter uncertainties and to determine the upper (or lower) 95 value of the response parameter.

The 2σ perturbations for the design and operating parameters are obtained from specifications, production characterizations, or operating limits. The 2σ model perturbation is derived from the PRIME qualification results and consists of an [[

]] Because the model perturbations are derived directly from the PRIME qualification results for the response parameter of interest, they address uncertainties in PRIME component models.

Additionally, because the model uncertainty is applied [[

]]

NEDC-33258P – Application Methodology

RAI-32 (full text)

Section 3.4.1 of NEDC-33258P describes how the critical pressure is calculated by perturbing various properties (cladding creep rate, cladding thickness, temperature, and pellet swelling rate). Please provide an example calculation of critical pressure mean value and bounding value with standard deviation. In addition, please provide justification (i.e., data) for the values used for the uncertainties in swelling, creep and temperature.

RAI-32 Supplement 1 (full text)

Provide an example of critical pressure calculation. Also describe the uncertainty for the fuel pellet swelling rate and cladding creep rate used in the critical pressure calculation.

Combined Response:

For GNF fuel designs, compliance with fuel rod thermal-mechanical licensing criteria is confirmed using the PRIME code and associated application methodology. The licensing criterion applied to rod internal pressure is to assure with 95% confidence that the pressure will not exceed the pressure at which the cladding creepout rate is equal to the pellet fission product swelling rate. This pressure is denoted the critical pressure. The criterion is applied to assure that cladding liftoff and the adverse feedback of liftoff on fuel temperature, fission gas release and rod internal pressure are precluded.

The method used to assure compliance with the criterion is [[

]]

A value of DR < 1 assures with 95% confidence that cladding liftoff will not occur. [[

]]Calculation of P_c and σ_{pc} are described below.

Relation for Critical Pressure

The expression for critical pressure is derived by [[

]]The derivation and resulting expression for critical pressure, using the PRIME creep correlation, are summarized in Attachment 2. From this derivation, [[

]] The bases for the swelling rate and creep correlation and associated uncertainties are as follows.

Pellet Swelling Rate and Uncertainty

As noted in the PRIME LTR, GNF assumes a nominal swelling rate of [[

]] As documented in a separate response, cladding profilometry of GNF commercial rods confirm that PRIME cladding strain predictions at high exposure using this swelling rate agree well with measured strains.

Attachment 1 includes Figures 1-1 through 1-4 provides information for the discussion of pellet swelling. [[

]] New GNF data as summarized in Figure 1-4 of Attachment 1 suggests that for burnup greater than [[

]] The revised rate is consistent with rates reported in the open literature, as summarized in Attachment 1. These observations support the use of the higher rate in the calculation of critical pressure for cladding liftoff.

For the calculation of σ_{pc} GNF has historically assumed a swelling rate uncertainty of [[ ]] As for the nominal swelling rate, this value was derived from GNF swelling measurements at relatively low exposure. As noted above new GNF high exposure swelling data [[ ]] This revised rate [[ ]] maintains some conservatism relative to the swelling rates reported in the open literature, as summarized in Attachment 1.

Cladding Creep Rate and Uncertainty

The relation for P_c derived in Attachment 2 assumes the same cladding creep correlation used in the PRIME code. The PRIME creep relation is expressed as a function of stress for 3 stress regimes - low, intermediate and high. [[ ]] For GNF 10x10 fuel designs, nominal values of critical pressure calculated using the relation derived in Attachment 2 correspond to cladding [[ ]] Thus the critical pressure calculation involves cladding stresses that are in the low stress regime for typical operating conditions. Based upon a comparison of the PRIME low stress creep correlation with the database, the uncertainty in the cladding creep correlation is taken to be [[ ]]

Critical Pressure and Uncertainty

To demonstrate the results of the swelling rate and creep correlation and associated uncertainties discussed above, typical results for the critical pressure and critical pressure uncertainty for a typical 10x10 design are presented below.

The critical pressure is calculated by applying the relation for P_c in Attachment 2. The critical pressure uncertainty is calculated by perturbing parameters used in the calculation of P_c on the basis of characterized uncertainties to determine the sensitivity of P_c to these parameters[[ ]] The methodology is described in NEDC-33258P.

For the typical 10x10 design, the most limiting point in terms of internal pressure design ratio occurs for the full length UO_2 rod at approximately end of life exposure. At this point, values of LHGR, T_k, Po and ϕ at the limiting axial node are

[[

]]

In summary, for a typical 10x10design at the most limiting point in terms of internal pressure design ratio, the cladding critical pressure is [[ ]] and the critical pressure uncertainty is [[ ]] Of the uncertainty, [[

]]

Attachment 1
Assessment of Swelling Data

[[ ]]

Figure 1-1: GSTRM Fuel Swelling Model (fuel column length change measurements)

[[ ]]

Figure 1-2: GSTRM Fuel Swelling Model (fuel density measurements)

[[ ]]
Figure 1-3: New GNF Measured Pellet Density Data from Three Different NUPEC Programs for 8x8 BWR Fuel.

[[ ]]
Figure 1-4: New GNF Swelling Data Derived from Pellet Density Measurements from Three Different NUPEC programs for 8x8 BWR Fuel.

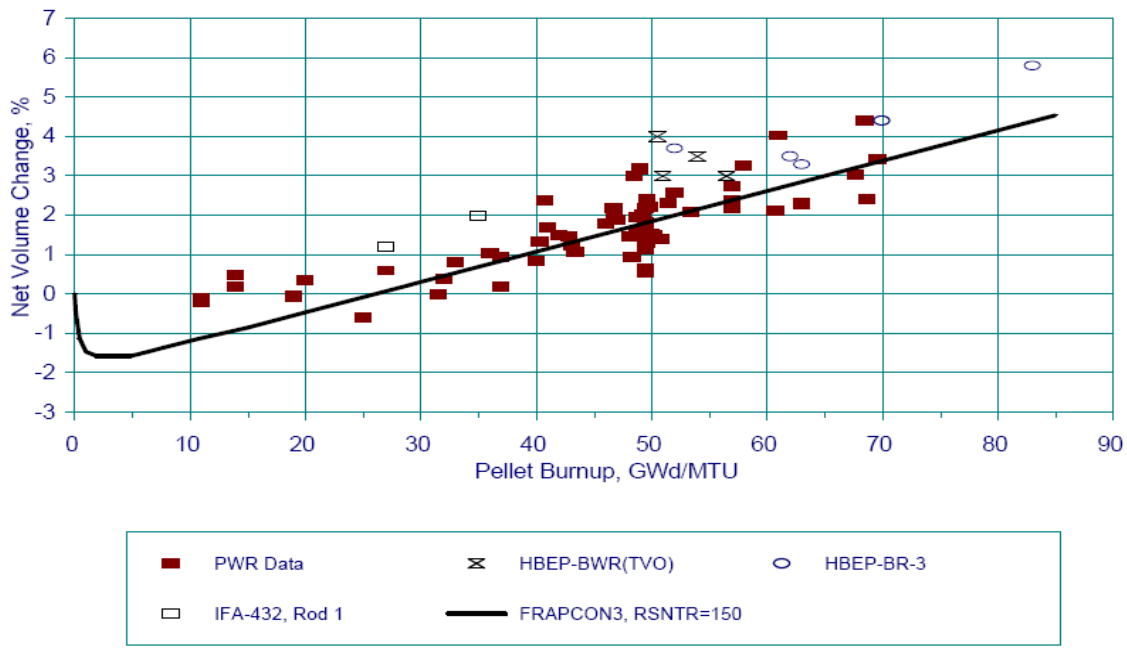

Figure 1-5: FRAPCON3 Fuel Swelling Model[1-1]

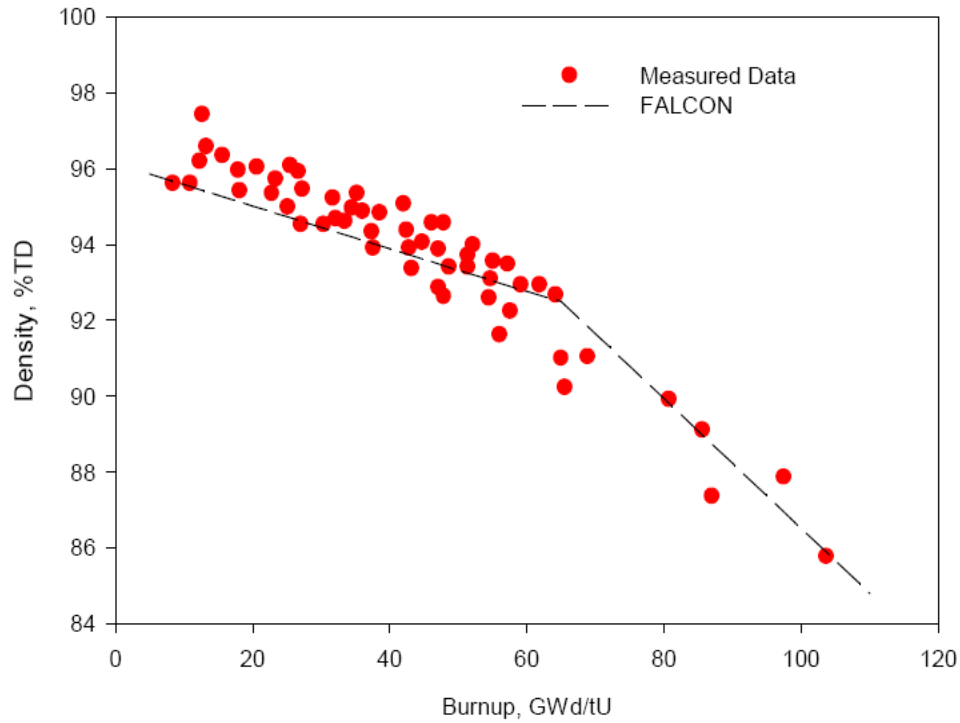

Figure 1-6: FALCON MOD01 Fuel Swelling Model[1-2]

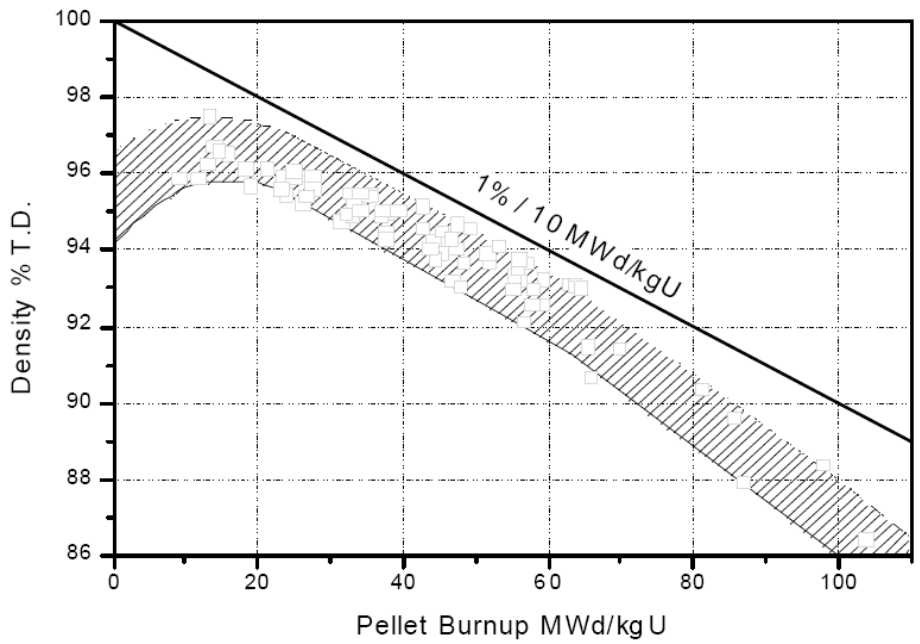

Figure 1-7: Density of Fuel Pellet as a Function of Pellet Burnup[1-3]

References:

[1-1] Lanning et. Al., "FRAPCON-3: Modifications to Fuel Rod Material Properties and Performance Models for High-Burnup Application", NUREG/CR-6534, October 1997.

[1-2] Lyon et. Al., "Capabilities of the FALCON Steady State and Transient Fuel Performance Code" Paper 1090, 2004 LWR Fuel Performance Mtg, Orlando, Florida

[1-3] Manzel R., "High Burnup Fuel Microstructure and its Effect on Fuel Rod Performance," 2000 Light Water Reactor Conference, Park City, Utah.

Attachment 2
Critical Pressure Relations with PRIME Creep Relations

For low stress irradiation creep, the generalized steady state strain rate is given as

[[

]]

[[

]]

Where P_c is in ksia

RAI-32 Supplement 2 (follow-up question)

Provide the rod internal pressure uncertainty used in the cladding lift-off calculations. Also discuss the recently published (May 2008 HPG Meeting) IFA-610.10 test observations with respect to the calculated critical pressure for GNF fuel design.

Response:

GNF provided the details about the critical pressure calculation and associated uncertainties in the RAI-32 S01 response. As noted in that response, GNF calculates the internal pressure design ratio DR as follows to assure with 95% confidence that the pressure will not exceed the pressure at which the cladding creepout rate is equal to the pellet fission product swelling rate. [[

]]

The values of P_i and σ_{pi} are obtained directly from the PRIME statistical licensing analyses. In response to RAI-38(a), GNF provided PRIME results for the maximum pressure case for a typical 10x10 fuel rod. The maximum rod internal pressure calculated is [[ ]] From the PRIME statistical analysis (which includes model uncertainty and geometric tolerances and operating uncertainties) the uncertainty in the rod internal pressure is determined, which is [[~]] [[

]]. A sample calculation for these values and associated uncertainties are provided in the RAI-32 S01 response. For completeness the numerical values for the Pc [[ ]] are repeated here. It is noted that the values of P_i noted above is from non-barrier cladding. The response to RAI-38(a) assumed non-barrier cladding to permit direct comparison of PRIME and FRAPCON results.

<u>Issues about Recently Published IFA610.10 test observations</u>

Based upon results presented at the recent 2008 Halden meeting, as documented in a presentation forwarded by GNF to PNNL, GNF concludes that liftoff, as indicated by a change in temperature [[ ]]. This is based upon data for the second test cycle. [[

]]Even if liftoff is taken to begin for a change in temperature [[ ]]based upon the average of results for tests IFA-610.1 and IFA-610.10 2nd cycle. This value is [[

]] determined by GNF and significantly higher than the effective lower bound value of [[ ]]calculated by GNF. Based upon HWR-877, which includes data for only the first test cycle, PNNL concludes that liftoff begins at an overpressure of [[ ]] This corresponds to a critical pressure of [[ ]]. The data in the presentation, which appears to indicate [[

]]

<u>Other Concerns:</u>

1. In the Halden presentation on IFA-610.10, a systematic increase in fuel temperature with exposure is attributed to liftoff. Possible causes of the temperature increase in addition to liftoff include

[[

]]

These items may be sufficient to explain the apparent liftoff for the second test cycle. If so, there would be no actual cladding liftoff, which would be consistent with no measured change in hydraulic diameter at hot standby. Assessments of some of the effects above for the first test cycle are included in HWR-877. Assessment for the second test cycle is not yet documented.

2. The fast flux is stated qualitatively to be applicable to BWR liftoff conditions. If the fast flux is only slightly different than the flux for BWR liftoff conditions, this could impact interpretation of the test results.

RAI-32 Supplement 3 (full-text)

In order to assess the overall conservatism of the NCLO methods, we need to fully understand the inputs and modelling uncertainties in the nominal Pcrit calculation. RAI 32 S01 (May 23) provides an "example" calculation. We need to know whether GNF feels that they have any degrees of freedom in selecting input and/or uncertainties relative to those documented in this RAI response. It would be best if this RAI was beefed up to specify which inputs and assumptions are part of the approved Pcrit methodology.

Response:

The fuel rod internal pressure design ratio calculation combines rod internal pressure and critical pressure statistical distributions (nominal value and standard deviation) to assure with 95% confidence that cladding liftoff will not occur.

As discussed in the response to RAI 32 S01, the rod internal pressure distribution is calculated using the PRIME statistical application methodology. The nominal internal pressure includes substantial conservatism due to the assumption of operation on a bounding LHGR limits curve. The internal pressure standard deviation is determined by the PRIME model uncertainty and uncertainties in fabrication, design and operating variables. The PRIME model uncertainty is determined from the PRIME qualification. The uncertainties in fabrication and design variables are determined from manufacturing specifications or production characterizations; the uncertainties in operating variables, which is taken to include cladding oxidation and crud responses, are determined from plant operating characteristics or fuel inspections. [[

]]

The critical pressure distribution is calculated using a relation derived by calculating the rod internal pressure required for the cladding creepout rate to be equal to the pellet swelling rate. The nominal critical pressure is determined largely by the cladding creep response and the pellet swelling rate. The cladding creep response is determined from the PRIME creep relations, as documented in Part 1 of the PRIME LTR, and is a function of hoop stress, temperature and fast flux. The hoop stress in turn is a function of cladding thickness, rod internal pressure and system pressure. The pellet swelling rate is assumed to be [[ ]] on the basis of the data discussed in the response to RAI 32 S01. Other inputs to the nominal critical pressure calculation include the following:

[[

]]

The values of these inputs are determined from PRIME inputs or outputs.

The critical pressure standard deviation is determined by the pellet swelling rate uncertainty, the cladding creep response uncertainty and the uncertainties in the other inputs noted above. The pellet swelling rate uncertainty is assumed to be [[ ]]on the basis of data discussed in the response to RAI 32 S01. Similarly, the cladding creep response uncertainty is taken to be [[ ]] on the basis of data discussed in the response to RAI 32 S01. The uncertainties in the other inputs are taken to be the uncertainties used in the PRIME fuel rod internal pressure statistical analysis. [[

]]

After NRC acceptance of the PRIME code and its associated statistical application methodology, acceptance of the nominal pellet swelling rate and swelling rate uncertainty noted above and acceptance of a creep response uncertainty, the approved parameters and uncertainties will be incorporated into the GNF fuel rod design and licensing methodology.

RAI-32 Supplement 04 (full text)

Please discuss how the PRIME model uncertainty and cladding creep rate uncertainties are applied in the critical pressure calculation for the compliance with the no cladding liftoff criteria.

Response:

The impact of the PRIME model uncertainty on the critical pressure calculation is summarized below (a more detailed discussion was included in the RAI-32 S03 response).

The fuel rod internal pressure design ratio calculation combines rod internal pressure and critical pressure statistical distributions (nominal value and standard deviation) to assure with 95% confidence that cladding liftoff will not occur.

The rod internal pressure distribution is calculated directly using the PRIME code. The internal pressure standard deviation is determined by the PRIME model uncertainty and uncertainties in design and operating variables. [[

]]

The critical pressure distribution is [[

]] [[

]]The pellet swelling rate is assumed to be [[ ]]on the basis of the data discussed in the response to RAI 32 S01.

Similarly, the critical pressure standard deviation is calculated independently of the PRIME code using the relation for critical pressure as provided in the RAI 32 S01 response. The uncertainties in the inputs to the critical pressure calculation are used in the relation for critical pressure to calculate numerically the partial derivative of critical pressure to each input. The partial derivatives are combined to determine the critical pressure standard deviation. With the exception of pellet swelling rate uncertainty and cladding creep rate uncertainty, the uncertainties in the inputs are taken to be the uncertainties used in the PRIME fuel rod internal pressure statistical analysis. The pellet swelling rate uncertainty is [[
]] on the basis of data discussed in the response to RAI 32 S01. Similarly, the cladding creep response uncertainty is taken to be [[ ]].

[[

]]However, [[

]]

In summary, the critical pressure uncertainty is determined from [[

]]

Supplement to RAI-32, S01, S02, S03 and S04 Responses

The above responses are based upon the current PRIME code and the current critical pressure calculation methodology. During discussions concerning the critical pressure, the NRC expressed concerns that [[

]]GNF has performed an assessment of the impact of the use of a low stress creep relation based upon thin shell theory in the PRIME code and of the impact of the use of thin shell theory in the critical pressure calculation. This assessment is included as Attachment 1 to this supplement.

Based upon this assessment, GNF concluded that [[

]]

However, [[

]] Additionally, [[
]] These changes will impact the critical pressure relation in Attachment 2 to the combined response to RAI-32 and RAI-32 Supplement 1 through the impacts on the expression for tangential creep rate and the expression for tangential stress, which is currently based on thin shell theory. The magnitude of the impact for a specific case is quantified in Attachment A.

The PRIME qualification will be repeated and new model perturbations will be derived based upon the results of the re-qualification. Section 5.6.1 of NEDC-33256P (PRIME Technical Basis), which describes the PRIME low stress creep relations for annealed cladding, will be revised to reflect the modified creep relation in the –A version of the PRIME LTR. Sections 2.0, 3.0, 4.0 and 5.0 NEDC-33257P (PRIME Qualification) will be revised to document the results of the re-qualification in the –A version of the LTR. Section 3.2.4 of NEDC-33258P (PRIME Application Methodology) will be revised to reflect the new model perturbations in the –A version of the LTR. All revisions to figures and text in the LTR will be included in the -A version of the LTR.

GNF will apply the modified PRIME code and resulting model uncertainties in fuel design and licensing calculations.

ATTACHMENT A

Assessment of Impact of Thick versus Thin Shell Relations

Introduction:

Historically, due to typical cladding geometries and the simplicity of fuel performance mechanical analyses, thin shell relations have been used to derive and apply cladding (Zircaloy) creep relations in fuel performance assessments. With the development of the PRIME code, which utilizes the finite element methodology, and thus models the cladding with the finite element equivalent of thick shell relations, the use of creep relations derived using thin shell theory was reevaluated. The conclusion was that [[

]]
GNF has recently submitted the PRIME code for NRC review. The purpose of this analysis is to assess the impact of the use of thin shell based cladding creep relations in the PRIME code and to assess the impact of thick versus thin shell relations on cladding liftoff calculations. As a result of this analysis, [[

]] However, [[

]] The analysis is summarized below.

Impact on Creep Relations

The current PRIME creep relations for annealed Zircaloy cladding consist of creep relations for [[

]]
To characterize the impact of the use of [[

]] This data is the newest, most prototypical and best characterized creep data for GNF annealed Zircaloy cladding under liftoff conditions. The radial, tangential and axial stress components, generalized stress, and ratio of tangential/generalized creep are calculated for each [[ ]]point using thick shell relations. The results are shown in Table 1, together with the corresponding quantities calculated using thin shell relations.

The [[

]]

Thus the current steady state[[

]] points yields

[[ ]]

From the results in Table 1 it is noted that using the average value of [[

]]

Table 1
Stress and Strain Calculations for K5 Creep Data
[[

]]

Impact on Liftoff Calculations

The licensing criterion applied to rod internal pressure is to assure with [[

]]
The cladding creep response under [[

]]

From typical [[

]]

Table 2
Stress and Strain Calculations for Typical 10x10 Cladding Liftoff Conditions

	Thin Shell	Thick Shell
[[		
		{3}]]

The results from Table 2 are used to transform the relations for generalized creep rate above to tangential creep rate. Details are presented in Attachment B and summarized below.

For thin shell relations the result is

[[

]]
Based upon this result, it is concluded that [[

]]

Impact on PRIME Analyses

To assess the impact of the modified [[

]]are shown in Table 3.

From Table 3 it is noted that the impact of the [[

]]

From Table 3 it is also noted that the impact [[

]]

Table 3a
Typical 10x10 Rod Internal Pressure & Cladding Creepdown Analysis Results

	PRIME03A	Modified PRIME03A
Rod Internal Pressure (psia)		
[[		
		]]

Table 3b
Typcial 10x10 Cladding Midplane Plastic Strain Analysis

	PRIME03A	Modified PRIME03A
Delta Plastic Strain, %		
[[		
		]]

Conclusions

Cladding creepdown during low exposure operation and liftoff during high exposure operation are determined by the steady state low stress, fast flux activated relation. The current PRIME steady state low stress, fast flux activated creep relation for annealed Zircaloy cladding was derived primarily from creep data obtained from pressurized tubes using thin shell stress relations. The geometries of the tubes were such that use of thin shell theory is an approximation. The impact of the approximation has been assessed by rederiving the relation for the most

prototypical data using thick shell stress relations and then (1) quantifying the impact on the liftoff calculation for typical GNF 10x10 fuel and (2) incorporating the modified relation into PRIME and repeating PRIME internal pressure and cladding permanent strain analyses for typical GNF 10x10 fuel.

The impact of rederiving the cladding steady state low stress, fast flux activated creep relation is to reduce the generalized creep rate to approximately [[

]]
For both liftoff and PRIME analyses, the differences are small both in an absolute sense and relative to the PRIME model uncertainty.

On the basis of this assessment GNF concludes that use of [[

]]However, as noted before, [[

]]

ATTACHMENT B

Impact of Thick/Thin Relations on Liftoff for Typical 10x10 Cladding

[[

]]

NEDC-33258P – Application Methodology

RAI-33 (full text)

The correlation for fuel enthalpy given in Section 3.3.5 of NEDC-33256P does not include a term to account for the heat of melting. Please describe any accidents or transients that PRIME will be used for that may include fuel melting along with the burnup level that fuel melting is experienced and the impact of fuel melting on future operation of the fuel rod. Please provide verification data with fuel melting that demonstrates PRIME adequately predicts the impact of fuel melting during the transient and operation following the transient (assuming no fuel failure).

Response:

The current PRIME application methodology [[
]]. However, GNF has performed tests to confirm the acceptable performance of fuel with melting in terms of redistribution of molten fuel. Summary of these tests are provided in the RAI 1.b response. [[

]]

NEDC-33258P – Application Methodology

RAI-34 (full text)

No model for cladding corrosion thickness is described. Page 3-5 of NEDC-33258P implies that corrosion thickness is input. Please provide more detail on how corrosion is input as well as a description of the current GNF corrosion model shown in Figure 3-1. Please identify the different fuel designs associated with the data in Figure 3-1.

Response:

The data in Figure 3-1 is liftoff data. [[

]]is plotted in Figure 3-1. PIE metallography has confirmed that liftoff conservatively indicates oxide thickness.

The liftoff data in Figure 3-1 is used to derive the 'corrosion' model used in PRIME. [[

]] from Figure 3-1 and then applied directly as inputs to PRIME analyses.

The data in Figure 3-1 was obtained from modern GNF fuel cladding operating in plants without water chemistry excursions or abnormal corrosion events. The basis for Figure 3-1, was discussed in detail during the February 12-13, 2008 NRC/GEH meeting and is documented in the Addendum to the Response to ESBWR RAI 4.2-2 and 4.2-4.

RAI-34 Supplement 1 (full text)

Please provide a specific example of how an oxide and crud thickness would be applied to a plant with an abnormal corrosion event, this RAI related to RAI2.

Response:

Normal PRIME design and licensing calculations are performed using the option (ICROX=1) in which [[ ]]The input vales are based upon crud and oxide measurements for plants with normal water chemistry. The nominal oxide thickness is defined in the supplemental response to ESBWR RAIs 4.2-2 and 4.2-4. The oxide conductivity is specified to be [[ ]] The nominal crud thickness and conductivity are defined in the response to RAI-2.

For abnormal corrosion events, involving either abnormal oxidation or crud buildup, PRIME assessments are performed in either of two ways. The first is to utilize the standard approach above [[ ]], as based upon in-pool and/or PIE results. Additionally, depending upon the characteristics of the crud layer, there is an option (ICRUD=0) to permit [[ ]]. For recent assessments involving tenacious crud, conductivities in the range of [[ ]] have been used. Finally, if the kinetics of either crud or oxide buildup are not linear, there is an option (ICROX=0) that permits step-by-step [[ ]]

NEDC-33258P – Application Methodology

RAI-35 (full text)

Figures 3-3, 3-5, 3-7, and 3-9 of NEDC-33258P demonstrate the upper 2s model predictions. However, in the application methodology, a 1.645s value is used. Please provide plots similar to Figures 3-3, 3-5, 3-7, and 3-9 that demonstrate that the upper 1.645s bounds 95% of the data with 95% confidence level.

Response:

As discussed in the response to RAI-31, the statistical analysis methodology includes a 2 sigma model perturbation, which also addresses [[ ]]. The result of this perturbation and the other 2 sigma perturbations are used [[ ]]. This uncertainty is then used to determine the upper or lower 95 (1.645 sigma) value for comparison to the licensing criteria.

NEDC-33258P – Application Methodology

RAI-36 (full text)

Figure 3-9 of NEDC-33258P demonstrates that the 2s model perturbation does not bound the diametral strain data. Please justify this behavior and if necessary, propose an additional uncertainty on cladding creepdown to bound 95% of this data with 95% confidence level.

Response:

The underprediction is considered in the context of the type of operation and measurement uncertainty for the data that is underpredicted and the analyses that include the model perturbation. The underpredicted data is obtained from profilometery of long term irradiations at low power and without power ramps. The predicted cladding deformations are within the uncertainty of the profilometry measurements. The model uncertainty is applied to fuel temperature and rod internal pressure analyses, where the 'underprediction' results in increased conservatism due to lower gap conductance. The cladding strain calculations are performed on a worst tolerance basis, which is equivalent to more than a 2 sigma perturbation. The ramp data in Figure 3-9 is generally bounded by the 2 sigma perturbation.

RAI-36 Supplement 01 (summary text)

As the cladding strain licensing calculations are preformed on worst tolerance basis, demonstrate that PRIME bound the diametral strain qualification cases on a worst tolerance basis. Separate out the ramp tests with a different color than the base irradiation case.

Response:

In Part 3 of the PRIME LTR (Application Methodology), the cladding diametral qualification results were replotted with the 2σ model perturbation used in the statistical methodology to calculate fuel temperature and rod internal pressure. The results indicated that slightly more than [[ ]]

However, as discussed during the meeting on May 1-2, 2008 the power histories used in the GNF analyses to determine the overpower to the cladding strain limit are similar to histories for the ramp test data in the qualification results and are performed on a worst tolerance basis. To address these issues relative to the PRIME qualification, the nominal qualification results were replotted with ramp test and steady state data differentiated. The results are shown in Figure 36. 1 and indicate that the ramp test data is generally overpredicted.

[[ ]]

Figure 36.1: PRIME Cladding Diametral Strain Qualification (Nominal)

The PRIME experimental qualification results were also redone with the [[ ]] licensing analyses. Because of limited information concerning the design and fabrication tolerances for the rods in the experimental qualification, only the perturbations expected to have a significant impact on calculated cladding strain were perturbed, and the perturbations were based upon GNF specifications and tolerances. The perturbations are defined in Table 36.1.

Table 36. 1: Perturbations for [[ ]]Analyses

Parameter	Perturbed Value
Pellet OD	[[
Clad ID	
Clad thickness	
Pellet density	
Pellet densification	
Oxide (Upper 2σ)	
Crud (Upper 2σ)	]]

It is noted that the GNF [[ ]]analyses include a factor of [[ ]] on LHGR to account for the possibility of power spiking due to fuel densification. This factor is conservatively applied even though densification is assumed to be zero in the cladding strain licensing analyses. This factor was not included in the reanalysis of the qualification results to permit better assessment of the conservatism in [[ ]]analysis methodology.

The results of [[ ]]qualification analyses are shown in Figure 36.2. From Figure 36.2 it is noted that all ramp test data is [[ ]]. For ramp test data with measured cladding diametral strain in the range of [[ ]] which is most pertinent to the licensing analyses to determine allowable overpower to the cladding strain limit, the [[ ]]on average. From Figure 36.2, it is also noted that for the steady state cases with measured strains greater than zero that the [[ ]]analyses yields [[ ]] of cladding diametral strain. Finally, from Figure 36.2 it is noted that while the [[analyses generally increase predicted strains for steady state cases with measured strains less than zero that for some of the cases the predicted strains are actually reduced, increasing the underprediction for these cases. This is as expected, since these cases tend to be in the moderate exposure range where the reduction in cladding thickness will increase the cladding creep down prior to pellet clad contact, which even with the reduced gap may not occur or may occur near the end of irradiation for the rods in these cases.

In summary, the results of the [[ ]]analyses confirm that [[ ]]y results in overprediction of cladding diametral strain for ramp test data and steady state data with measured [[ ]], and meets the intent of the methodology to provide conservative cladding strains for PRIME licensing analyses.

[[ ]]

Figure 36. 2: PRIME Cladding Diametral Strain Qualification (Worst Tolerance)

NEDC-33258P – Application Methodology

RAI-37 (full text)

Figure 3-10 of NEDC-33258P shows a typical design basis power versus exposure envelope. This figure only goes to 70 MWd/kgU. Approval for PRIME is being sought to 80 MWd/kgU. Please provide a typical design basis power versus exposure envelope to 80 MWd/kgU.

Response:

The operating limits for GNF fuel designs are specified as envelopes of [[ ]]. These envelopes are specified to meet the competing requirements of [[ ]]. [[ ]]The typical LHGR limits envelope in Figure 3-10 is for the GE14 UO_2 rod. The first GNF fuel design that will go beyond [[ ]]fuel design. The proposed LHGR limits for this design for the UO_2 rod are shown in Figure 37.1.

]]

[[ ]]

Figure 37.1: GNF2 UO2 LHGR Limit up to [[ ]]

NEDC-33258P – Application Methodology

RAI-38 (full text)

PNNL would like to perform audit calculations comparing PRIME results to results from FRAPCON-3. Please provide tabulated input and output values for the following cases to allow audit analyses to reproduce output using a typical 10x10 rod.

a. *Maximum pressure case at LHGR limit showing fuel centerline temperature, burnup, pressure, void volume, and FGR as a function of input time for each time step.*
b. *Realistic maximum power history cases with typical AOO transients applied at 30, 40 and 50 GWd/MTU showing peak fuel centerline temperature burnup, pressure and FGR as a function of input time.*
c. *Maximum strain increment case with typical AOO transient showing fuel centerline temperature, burnup, total strain (elastic+plastic), permanent strain, and gap size (or interface pressure) as a function of input time*
d. *Maximum temperature case with typical AOO transients applied at 30, 40, and 50 GWd/MTU showing burnup and centerline temperature as a function of input time. If this case is the same as requested in part b, combine with the results from part b.*
e. *Please provide a sample calculation for a LOCA initialization calculation including code input and that output that is relevant to the LOCA calculation.*

Response:

The requested inputs and PRIME results for the audit calculations are included in the attached data package (Reference 38.1). During the tabulation of the results for RAI-38.c, very low cladding permanent strain compared to the licensing limit of 1% was noted for the most limiting exposure [[ ]] for the realistic [[ ]] case. To permit code comparison for cases with the strain approaching the licensing limit, results for [[ ]] cases are also included in the attached data package.

Reference:

[38.1] MFN 09-106 Supplement 1, Data Package

NRC RAI-39 (full text)

TRACG employs both GSTRM and PRIME fuel performance models. NRO's review of TRACG deferred approval of the PRIME model and uncertainty applications. Which means that our review of PRIME must include this application. GEH will need to submit a detailed description of the use of PRIME models within TRACG and justify the uncertainties applied in the transient analyses. Particular attention needs to be focused on the relative change in predicted parameters. Since the dynamic fuel temperature calculation (i.e. change in temperature) directly impacts fuel doppler reactivity feedback (first order impact on transient analyses), this relative effect needs to be investigated.

RAI-39 Supplement 1 (full text)

What is the impact on LOCA PCT and oxidation due to a factor of 10 higher gap conductance (ratio of FRAPCON/PRIME value) and a 50% lower rod pressure than the LOCA input from PRIME.

RAI-39 Supplement 2 (full text)

The response to the downstream impacts RAI will include TRACG04 sensitivity analyses using both PRIME and GSTRM models. The analyses will quantify the differences in the safety analysis figures of merit based on the differences in the respective TM models. These figures of merit will include all relevant analysis outputs or appropriate surrogate outputs to address the complete body of analysis of record. In other words, these analyses should address: DCPR/ICPR, plastic strain, and fuel centerline temperature for AOOs; PCT, oxidation, and hydrogen formation for LOCAs; PCT, water level, suppression pool temperature, and peak vessel pressure for ATWS; and regional, core wide, and channel decay ratio and growth rate for stability.

The results of the sensitivity analyses will be provided for the staff to assess any significant impact of the continued use of the GSTRM based transient analysis methods after the introduction of PRIME. The staff review of the RAI response will be documented in the PRIME SE. If necessary the staff will determine if additional margin is required to address these sensitivities based on the results and apply conditions or limitations as appropriate until such time as the code stream is upgraded to be consistent with the PRIME models.

Please address the planned implementation of PRIME and the necessary upgrade of the downstream safety analysis codes to incorporate the PRIME model. These safety analysis codes include, but are not necessarily limited to: ODYN, ODYSY, TASC, SAFER, CORECL, and TRACG.

Response

The NRC expressed concern that the PRIME code may under-predict the pellet to cladding gap conductance compared to the FRAPCON code. The initial results of the NRC/PNNL comparison indicated that PRIME calculates [[ ]] gap conductance than FRAPCON. It is noted that this ratio was derived by comparing FRAPCON gap conductance at the peak power node to PRIME axial node 3 gap conductance, as illustrated in Figure 39-1 "FRAPCON Peak/PRIME Node 3 Gap Conductance". However, in order to make a representative comparison between the codes, the gap conductance should be compared at corresponding peak power nodes. If the PRIME gap conductance at peak power nodes is compared with FRAPCON gap conductance at peak power nodes, the ratio between these two codes would be [[ ]] as previously reported. The comparison of the FRAPCON/PRIME peak-to-peak gap conductance is shown in Figure 39-1 "FRAPCON Peak/PRIME Peak Gap Conductance".

[[ ]]

Figure 39-1 Ratio of FRAPCON and PRIME Gap Conductance

Results from the requested TRACG04 sensitivity studies to assess how implementation of the PRIME impacts licensing parameters are summarized in Table 39-1. The more recent calculated results to represent the operating BWR fleet are shown in the upper half of the table. These results include a third calculation where the gap conductivity calculated by the PRIME03 models [[ ]] Relevant results selected from those provided previously for the ESBWR via MFN 08-713 (Reference 39-1) are near the end of the table. The

third calculation with the scaled-up gap conductivity was not performed for the earlier ESBWR analyses because the more recent calculations for operating BWRs clearly show that scaling-up the gap conductivity produces results that are essentially the same or are less conservative than using the PRIME models without the factor.

For purposes of implementation in TRACG04 the replacement of GSTRM models with PRIME03 models consists of two elements. Both elements are described in the *TRACG Model Description LTR,* NEDE-32176P, Rev. 4 (Reference 39-2) that has already been provided. The first and most important element is the [[

]] This change causes the [[

]] This information is provided to TRACG04 via the fuel files where it is tabulated as a function of exposure, LHGR history and instantaneous LHGR. The GSTRM and PRIME03 fuel files are similar in format and content but differ in the amount of fission gas that has been released from the fuel [[ ]]. Both model elements combine to result in a TRACG04 steady state condition where [[

]] This impact on average initial fuel temperature is shown in the table. Because the [[

]] If the gap is already closed, as is the usual case for the exposure conditions where the licensing parameters tend to be limiting, the initial contact pressure between the fuel pellet and the inner surface of the cladding will be higher. All these aspects are sources for the uncertainty as explained in Section C3BX in Chapter 5 of NEDE-32906P-A (Reference 39-3). The overall uncertainty determined previously to be [[

]] to be applied with the lower thermal conductivity values calculated by the PRIME03 model as indicated in NEDE-33083, Supplement 1 (Reference 39-4). The previously-approved application process allows the uncertainties to be recalculated without further NRC review and approval provided the same process is followed.

The following paragraphs discuss how changes in initial conditions and modeling impact the transient responses and licensing parameters for different scenarios.

For AOO transient analyses the licensing basis operating limit minimum critical power ratio (OLMCPR) is typically the licensing parameter that presents the greatest challenge. OLMCPR is usually set by a pressurization event so this is the kind of event that was analyzed. As anticipated and demonstrated in the table, the dome pressure and water level are not sensitive to changes in the fuel thermal conductivity. On the other hand, the peak powers during pressurization events are typically very sensitive to many different inputs, so peak powers are used as a *sensitivity gauge* even though they are not a licensing parameter and have essentially no influence on any of

the licensing parameters. Integrated power and the flow for the limiting channel are the most important parameters for determining ΔCPR/ICPR. Fuel thermal conductivity impacts Doppler and void feedback in complex ways so that the system response and limiting channel responses counter each other. Doppler feedback is stronger for higher initial fuel temperatures. Void feedback is stronger for higher gas conductivities and is weaker for reduced pellet thermal conductivities. Increasing the gap conductivity has the biggest impact on the fresher fuel earlier in the cycle where the gap is still open but has negligible impact on the ΔCPR/ICPR response determined by the fuel rods in the limiting channel since the gap has already closed before reaching the cycle exposure where ΔCPR/ICPR is the most limiting. Even when the gap is open no effect is seen for further increases in the gap gas conductivities beyond the point where the gap conductance is no longer the limiting thermal resistance in the heat transfer series from pellet to clad to coolant. Maximum fuel centerline temperatures for rapid AOO events are strongly influenced by the initial conditions so the trend for centerline temperatures for the three cases is similar to the trend in the average initial fuel temperatures. There is a substantial amount of margin to centerline melting [[

]].

TRACG04 currently does not report plastic strain in its output so the surrogate total strain was estimated using the hoop stresses and temperature calculated by TRACG04 at the limiting location and the elastic modulus calculated using the same correlation that is used in PRIME03. It is evident from the very low values for the ratio of hoop stress to yield stress (that TRACG04 does report) that the estimated total strains are essentially entirely elastic so that plastic strain can be assumed to be negligible.

The results in the table show that for fast AOO transients where the dynamic response associated with fuel thermal conductivity would be most evident, that the only licensing parameter that is impacted in a non-negligible way is centerline fuel temperature. The impact on all the other licensing parameters are essentially negligible and on the order of the uncertainties for the parameters. The added results from the BWR/4 AOO analysis confirm the results provided previously for the ESBWR.

Table 39-1 also contains key results for a core-wide stability case for a BWR/4 that has been added to supplement the ESBWR regional stability results provided previously. For both plant designs changing from the [[

]]. These results are typical of proportional reductions that have been seen in other stability studies to assess the PRIME03 downstream impacts. [[

]] Table 39-1 also shows that applying a factor to increase the

conductivity of fission gases in the gap works in the opposite direction for those fuel rods where the gap is still open.

Additional results for ATWS evaluations for operating BWRs were not generated because ESBWR evaluations provided previously confirm the expectation that the two licensing parameters, maximum vessel pressure and suppression pool temperature, are insensitive to changes in the details of how the fuel thermal conductivity is modeled. In ATWS scenarios the water level is being controlled by operator action and in any case has been shown by the AOO results to be insensitive to fuel thermal conductivity modeling. Sensitivities in peak clad temperature (PCT) for ATWS are similar in trend to those for LOCA. Differences in initial fuel temperatures are quickly washed out and are overshadowed by the power response which is dominated by hydraulic conditions.

Previously LOCA events were not addressed for the ESBWR because they are benign for that design so there is no need to address them here. Table 39-1 presents calculated results for design basis accident (DBA) LOCA results for the limiting BWR/4 and BWR/2 scenarios. Again the impact of the modeling change from GSTRM to PRIME03 on the average initial fuel temperature is seen. Differences in initial fuel temperature are largely irrelevant for the transient [[

]]. The longer term response in PCT is dominated by the balance between decay heat and ECCS cooling so it is insensitive to changes in modeling the fuel thermal conductivity. Oxidation of the cladding is an exponential function of clad temperature so as expected these quantities like the cladding temperatures are also insensitive to changes in modeling the fuel thermal conductivity. Oxide values are not reported for the BWR/4 calculations because they are negligible for these low PCT values. Note that the licensing requirement to limit the total core volume of oxidized zirconium to less than 1% is the means by which hydrogen production is maintained below an acceptable amount.

In conclusion, it has been shown that the primary impacts on transient licensing parameters of switching from [[

]] The impacts on all the other licensing parameters are essentially negligible and on the order of the uncertainties for these parameters.

Table 39-1 Summary Table

Description	GSTRM Baseline	PRIME03	PRIME03 with increased gap conductivity
Fuel conductivity model	GSTRM	PRIME03	PRIME03
Fuel file basis	GSTRM	PRIME03	PRIME03
Gap conductivity multiplier	[[		]]
BWR/4 AOO Turbine Trip without Bypass (TTNB)			
peak total power (%)	[[		
peak dome pressure (MPa)			
limiting ΔCPR/ICPR			
avg. initial fuel temperature (K)			
centerline temperature (K) melting temperature (K)			
max. ratio hoop stress to yield stress max. estimated total strain (%)			
min. NR water level (inches decreased from initial value)			]]
BWR/4 Core-wide Stability for a Limiting Case with Growing Oscillations			
decay (growth) ratio	[[		
avg. initial fuel temperature (K)			]]
Design Basis Accident LOCAs			
BWR/4 PCT (K)	[[		
avg. initial fuel temperature (K)			
BWR/2 PCT (K)			
avg. initial fuel temperature (K)			
max. cladding oxide: thickness (%) core volume(%)			]]
ESBWR AOO LRNBP (Reference 39-1)			
max. neutron flux (%)	[[		
peak dome pressure (MPa)			
limiting ΔCPR/ICPR		]]	
ESBWR ATWS from MSIVC (Reference 39-1)			
max. neutron flux (%)	[[		
max. vessel pressure (MPa)			
max. bulk suppression pool temperature (ºC)		]]	
ESBWR Regional Stability from LOFWH (Reference 39-1)			
peak total power (%)	[[		
decay ratio		]]	

Regarding the implementation of PRIME into the downstream codes.

In Reference 39-5, GEH documented the plan to provide a supplement to the GEH Licensing Topical Report, NEDC-33173P (IMLTR), describing the implementation of the PRIME model into the downstream safety analysis codes. That plan, as part of the IMLTR, would apply to future license applications for extended power uprate (EPU) and MELLLA+.

For GNF2 fuel applications and future fuel products, GEH will apply the PRIME code to thermal mechanical fuel design. After the downstream safety analysis codes are upgraded and the NRC issues their audit report, GEH will also utilize the downstream safety analysis codes with the PRIME inputs for GNF2 fuel applications and future fuel products. The -A version of the PRIME LTR will be revised to incorporate the NRC audit report.

References

39-1
Letter from RE Kingston (GEH) to Document Control Desk (USNRC), Docket No. 52-010, Subject: Response to Portion of NRC Request for Additional Information Letter No. 156 Related to ESBWR Design Certification Application - Emergency Core Cooling Systems - RAI Number 6.3-54 S01, MFN 08-713, September 22, 2008.

39-2
Letter from RE Kingston (GEH) to Document Control Desk (USNRC), Subject: Transmittal of GE Hitachi Nuclear Energy (GEH) Licensing Topical Report, NEDE-32176P, Revision 4, *TRACG Model Description*, January 2008, MFN 08-072, February 6, 2008.

39-3
GE Licensing Topical Report, "TRACG Application for Anticipated Operational Occurrences (AOO) Transient Analyses", NEDE-32906P-A, Revision 3, September 2006.

39-4
Letter from JC Kinsey (GEH) to Document Control Desk (USNRC), Docket No. 52-010, Subject: Transmittal of Accepted Version of Licensing Topical Report NEDE-33083P-A, Supplement 1, Revision 1, "TRACG Application for ESBWR Stability Analysis," January 2008, MFN 08-016, January 28, 2008.

39-5
Letter from JF Harrison (GEH) to Document Control Desk (USNRC), Subject: NEDC-33173P - Implementation of Limitation 12 (TAC No. MD0277), MFN 09-143, February 27, 2009.

RAI-40 (full text)

Provide details about the rain flow method and fatigue curve.

Response:

The fatigue life of many metals subjected to cyclic loading, including Zircaloy, is conveniently represented by the S-N curve, in which S represents the amplitude of the applied cyclic load and N represents the number of cycles required to cause failure at that amplitude. The GNF fatigue life data for Zircaloy is shown in Figure 40.1.

[[ ]]

Figure 40.1: Zircaloy Fatigue

For simple loadings consisting of a single amplitude centered about 0, the fatigue damage can be calculated using Miner's rule, in which the cumulate fatigue duty is taken as the ratio of the number of applied cycles at that amplitude to the number of cycles required to cause failure at that amplitude. Failure is taken to occur when the fatigue duty reaches 1.0. This concept can be applied to simple loadings consisting of more than a single amplitude if the amplitudes are each centered about 0. In this case, the cumulative fatigue duty is the summary of the duty due to the discrete amplitudes.

For complex loading consisting of variable amplitude cycles not centered about 0, the calculation of fatigue duty by direct application of Miner's rule is complex and subject to possible nonconservatisms. The rainflow cycle counting method was developed to eliminate the nonconservatism and still permit the application of Miner's rule. The method was developed by Matsuiski and Endo in 1968 ('Fatigue of Metals Subjected to Varying Stress', Japan Soc. Mech. Engrg, 1969) and has become the most generally accepted and widely applied method for calculation of fatigue duty for complex loadings.

In the rainflow method, the applied loading is reduced to a sequence of tensile peaks and compressive troughs. The time history is rotated 90 degrees and assumed to be a rigid roof. Half cycles are counted by imagining each tensile peak is imagined as a source of water that 'drips' down the roof until it terminates either by reaching the end of the time history, merging with flow that started at an earlier peak, or flowing opposite a tensile peak of greater magnitude. The process is repeated for compressive troughs. The magnitude of each half cycle is set equal to the difference in magnitude between the load at the start and the load at termination. A simple example is shown in Figure 40.2.

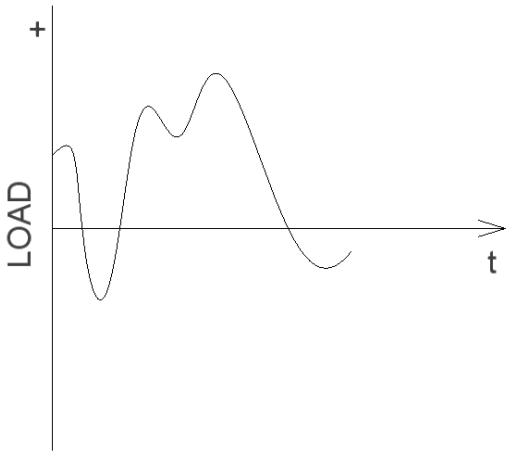

A) APPLIED LOADING

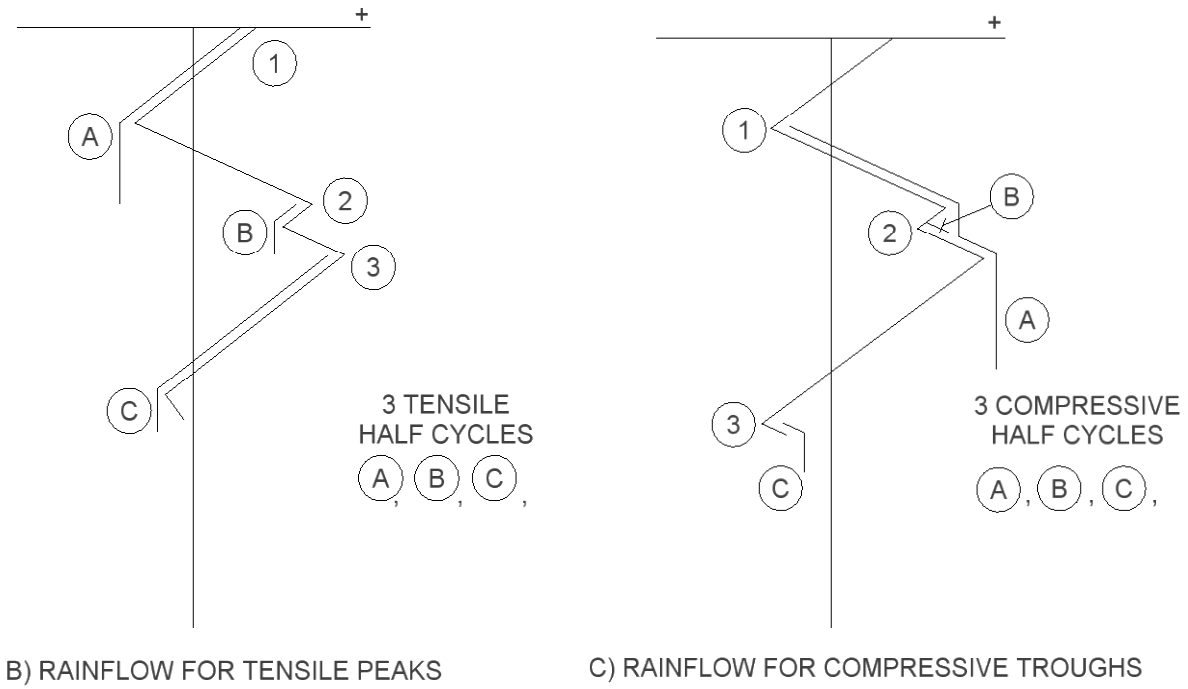

Figure 40.2: Rain Flow Fatigue Cycle

After determination of half cycles, half-cycles of equal magnitude but opposite sense are paired up to determine the number of cycles at each magnitude. Some residual half cycles are typically anticipated. The cumulate fatigue duty is then calculated by summing the fatigue duty due to the cycles determined as above using the S-N curve.

RAI-41 (full text)

Discuss in details how the plenum temperature is calculated for using as an input in PRIME.

Response:

GNF fuel designs include a plenum at the upper end of the rod above the fuel column (and in some designs at the lower end of the rod). The upper plenum contains a stainless expansion spring to prevent axial motion of fuel pellets during shipping and [[ ]]. The configuration is shown schematically in Figure 41.1.

[[ ]]

Figure 41.1: Typical Plenum Configuration

The plenum initially contains helium fill gas. During irradiation of the rod, fissions gases, primarily xenon and krypton and some helium, are released from the fuel and mix with the helium fill gas in the plenum. The temperature of the gas mixture in the plenum is determined as follows.

First, [[

]]

Next, heating rates in the cladding tube, canister and chips are used to perform heat transfer analyses to determine the temperatures of the chips, canister and cladding tube. [[

]]

[[

]]

The value used by GEN for thermal-mechanical analyses of the GE14 full length UO_2 and gadolinia rods is [[
]] These conservatisms are [[
]]

For part length rods, the results of the plenum gas temperature are different due to the plenum components being in a region of higher gamma heating and the top of the fuel column being in a region of higher power (and this higher temperature at the top of the column). These effects are specifically addressed for each part length rod design.